J. Fluid Mech. (1978), *vol.* 89, *part* 4, *pp.* 673–707
Printed in Great Britain

Buoyancy-induced flows in water under conditions in which density extrema may arise

By BENJAMIN GEBHART AND JOSEPH C. MOLLENDORF

Department of Mechanical Engineering, State University of New York, Buffalo

(Received 18 April 1977 and in revised form 31 October 1977)

The temperature dependence of the density of both pure and saline water, even to very high salinity and pressure levels, decreases at decreasing temperature toward an extremum. The nature of this variation precludes approximating the buoyancy-force density difference linearly with a temperature difference. This peculiar density variation of water has very significant effects, even at environmental temperature levels. A new equation has appeared which relates density to temperature, salinity and pressure with very high accuracy. Its form is especially suited to the analysis of convective motions. We consider here vertical boundary-layer flows. Analysis of flows arising from thermal buoyancy and from combined buoyancy effects shows the simplicity of the formulation. Relatively few new parameters arise. Extensive calculations for thermally buoyant flows show the large magnitude of the effects of the complicated density variation on transport. Buoyancy-force reversals and convective inversions are predicted. The latter are in close agreement with past experiments. A new Grashof number arises which is an accurate indication of the actual local flow vigour. The effects of specific temperature conditions are given in detail. The appreciable effect of the Prandtl number is calculated. Transport parameters are given for salinities and pressures up to 40 p.p.t. and 1000 bars, respectively.

1. Introduction

The density extremum in pure water at atmospheric pressure, at about 4 °C, is well known. An extremum also occurs in saline water, up to a salinity level s of about 26 p.p.t. (parts per thousand), and at elevated pressures up to about 300 bars abs. in pure water in local thermodynamic equilibrium. An extremum is also found well beyond these conditions in non-equilibrium circumstances. Figure 1 shows the variation of density with temperature in the vicinity of the density extremum for several salinities and pressures. The temperature at maximum density $t_m(s,p)$ is seen to decrease with increasing salinity and pressure, as does the equilibrium ice-melting temperature $t_{il}(s,p)$.

These ranges of temperature, salinity and pressure occur both in terrestrial waters and in many technological processes. In buoyancy-induced flows driven by differing temperatures near the extremum temperature, maximum-density conditions might arise and influence the motion. In fact, given the dependence of density on temperature, salinity and pressure and the dependence of the extremum temperature on both salinity and pressure, several density extrema may conceivably occur across a

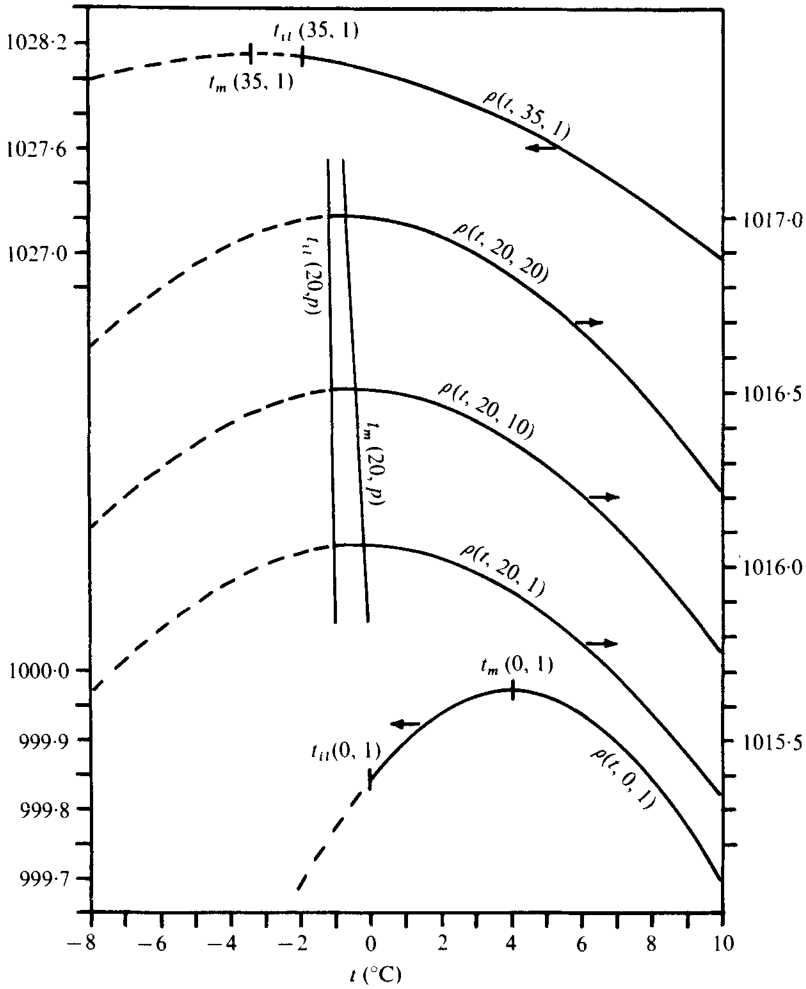

FIGURE 1. The density–temperature dependence at various s and p as formulated by Gebhart & Mollendorf (1977). $\rho(t, s, p)$ is in kg/m^3, t in °C, s in p.p.t. and p in bars abs. Also shown is the equilibrium phase interface and the temperature of maximum density. The arrow associated with each curve indicates the vertical scale which applies.

given flow region. That is, in a region of gradients of temperature, salinity and pressure, more than two trends in the density might arise. It is not always possible to ascertain the occurrence of extrema from the boundary conditions since interacting diffusive and convective processes determine the local density.

A general analysis of a particular flow geometry seems, initially, to be very complicated, even if the Boussinesq approximation is applied to the extent of neglecting density variations in continuity considerations. The problem arises in the buoyancy force $\mathbf{g}(\rho_r - \rho)$, where $\mathbf{g}$ is gravity, $\rho(t, s, p)$ is the local density and ρ_r is a local reference value, usually that which determines the local change in the hydrostatic pressure level p_h. The other part of the conventional approximation is the expression of this local density difference linearly in terms of the differences $t - t_r$ and $s - s_r$, using the respective volumetric coefficients of expansion as constant coefficients. This is not an attractive or often even a reasonable formulation when a density extremum condition arises, since the thermal expansion coefficient may then be positive, zero and negative within such a flow. The results would be very awkward; see, for example, the ice-melting results and observations of Bendell & Gebhart (1976).

However, as we shall see, we may dispense with this second approximation and retain comparable simplicity. This may be done in greater generality than in past work. We may cover a wide range of the most important conditions in which density extrema may occur. This may also be done for saline water and at pressure levels up to 1000 bars.

There are three kinds of buoyant convective motions: flows inside cavities; circulations, which may occur in horizontal and unstably stratified fluid layers; and external flows, which are caused in an extensive quiescent ambient medium by a localized temperature or salinity condition. We consider here only external flows in which density extrema may arise.

Such circulations have been considered both experimentally and analytically for spherical, cylindrical and flat surfaces in cold pure water. Apparently Codegone (1939) was the first to demonstrate convective reversals (or inversions) around the density extremum. Most subsequent experimental studies are reviewed by Bendell & Gebhart (1976). Several additional ones are discussed here in conjunction with their relation to analyses.

The first analysis of such motions known to us was done by Merk (1953). Using an integral method, he calculated the local heat transfer at low temperatures around a melting sphere. Convective inversion was predicted.

Schechter & Isbin (1958), using the buoyancy-force approximation developed by Merk, applied an integral method and an analog-solution technique to flow adjacent to a vertical surface in water at around 4 °C. The analysis led to a prediction, in terms of Chappius' density coefficients in the density expression used by Merk, of the actual flow direction. This work is interesting although it is not clear what unrealistic effects might arise from assuming conventional profiles. As we shall see, an integral analysis is especially suspect for these flows.

Goren (1966) considered a vertical surface at a temperature t_0 in ambient water whose temperature t_∞ was that of maximum density, i.e. $t_\infty = t_m$. The usual equations of motion were used with the buoyancy $\Delta\rho$ taken as $\rho_m \alpha(t-t_m)^2$, where

$$\alpha = 8{\cdot}0\times 10^{-6}(^\circ\mathrm{C})^{-2}$$

is a conventional value said to give sufficient accuracy for ± 4 °C around t_m. No additional parameters arise and an analog-computer solution was given for $Pr = 11{\cdot}4$. Vanier & Tien (1967) extended the study of Goren above its implied accuracy limit of $t_\infty = 8$ °C by approximating the driving density difference by a sum of linear, square and cubic terms in $t-t_m$, according to the density data of Perry (1963). This is similar to the treatment by Merk. The penalty in the analysis is two t_0-dependent parameters in two new terms in the differential equations. The formulation is still limited to $t_\infty = t_m$. Neglecting these terms, they repeated Goren's calculations and obtained values about 15% higher. Solutions were given for specific values in the range of $0 < t_0 < 35$ °C.

The measurements by Oborin (1967) on a sphere and horizontal cylinder in water agreed with Merk's prediction of convective inversion. The observations of Schenk & Schenkels (1968) for ice spheres in cold water were in fair agreement with the experimental results of Dumoré, Merk & Prins (1953) and with the analysis of Merk (1953). The minimum in the heat-transfer parameter was said to occur at $t_\infty = 5{\cdot}3$ °C, in better agreement with the prediction of Merk. Although the spread of the data seems too great to support such accuracy, these data are evidence of a reasonably well-defined convective inversion.

Vanier & Tien (1968) discussed in detail the directional tendencies of flow across the boundary region formed adjacent to a vertical surface in ambient water at temperatures around its density extremum. The effects of the relation of t_0 and t_∞ to t_m were outlined. The density formulation used by Merk was then used in an analysis. The equations were reduced to similarity form. However, additional parameters arose which depended on the three constants β_i in the density formulation and also on t_0 and t_∞. The sign of the buoyancy-force term must be changed according to a set of criteria. Numerical results for $t_\infty = 0$ and $1 \leqslant t_0 \leqslant 14$ °C were compared with the predictions of Schechter & Isbin. Considerable differences were found. Calculations were also made for other values of t_∞. However, the authors concluded that there are several temperature zones in which 'the physical model cannot accurately be applied'. Calculations were also compared with some of the data of Ede (1951) and of Schechter & Isbin, and showed fair agreement. The density formulation chosen imposes unfortunate limitations and complexity on the analysis.

Govindarajulu (1970) used the full equations, again with $\Delta\rho \propto (\Delta t)^2$, for water at $t_\infty = t_m$ to consider both vertical and horizontal porous surfaces. Similarity was formulated for a power-law downstream surface temperature variation $t_0(x)$ ($d = t_0 - t_\infty = Nx^n$ in our notation below). The required x dependence of the blowing velocity for similarity was given. No solutions were determined.

Roy (1972) re-solved Goren's problem and also obtained results which were different by about 15%. Then a large Prandtl number approximation was made to solve the problem by a method of inner and outer layers, even though water is the only prominent liquid of moderately high Prandtl number having a density extremum. Soundalgekar (1973) used the $\Delta\rho \propto (\Delta t)^2$ buoyancy formulation, again for $t_\infty = 4$ °C in an integral analysis and again with the conventional profiles also used by Schechter & Isbin, to calculate more simply the surface shear stress. Bendell & Gebhart (1976) have determined the melting rates of vertical ice slabs in ambient water at temperatures from about 2 to -20 °C. The results were converted to a heat-transfer parameter and are in very good agreement with calculations made by the present authors with the new formulation.

The previous studies of transport in water around its density extremum have been made for pure water at 1 atm. Experimental studies have been made for spheres, horizontal cylinders and vertical surfaces. Analytical work has used the buoyancy-force approximation of Merk or the other conventional one $\Delta\rho \propto (\Delta t)^2$. Integral analyses have been performed around a sphere and also adjacent to a vertical surface. All relatively simple analyses using the full equations have been one sided, in the sense of taking $t_\infty = t_m$, the extremum temperature. No buoyancy-force inversion then occurs in the convection region. The studies using a cubic polynomial for the density variation with temperature were faced with a number of additional problem particular parameters. This, as we shall see, is unnecessary.

The present work retains all first-order effects in a formulation which treats convection around a density extremum, for both pure and saline water, over a wide range of pressure levels. Similarity is achieved with a minimum of parameters. Also formulated is the full problem of the vertical boundary-layer regime with simultaneous diffusion of momentum, thermal energy and salinity for t_∞ and t_0 on either side of t_m. The accuracy of the buoyancy-force formulation will be that of the density relation $\rho(t, s, p)$ used to calculate it.

2. The formulation

The equations of steady laminar motion, with a Boussinesq approximation, in (1)–(4), and with constant molecular diffusion properties μ, k and D are

$$\nabla . \mathbf{w} = 0, \tag{1}$$

$$\rho_1(\mathbf{w} . \nabla)\mathbf{w} = \mathbf{F} - \nabla p + \mu\nabla^2\mathbf{w}, \tag{2}$$

$$\rho_1 c_p(\mathbf{w} . \nabla)t = k\nabla^2 t + \beta T(\mathbf{w} . \nabla)p + \mu\Phi, \tag{3}$$

$$(\mathbf{w} . \nabla)s = D\nabla^2 s, \tag{4}$$

where $\mathbf{F} = \mathbf{g}\rho$ is the body force per unit volume, p is the local static pressure and $\mathbf{w}$ is the local velocity of the centre of mass. The approximation used in (1) is much more accurate for the conditions relevant to this study than in general. Note that the form of (1) leaves the specific value of ρ_1 unspecified.

The salt concentration s is assumed small compared with the density of the water. We note that s for sea water is around 35 p.p.t. The formulation neglects distributed energy and salinity sources, e.g. from chemical reactions. The Soret effect is not included as it is a relatively small effect in the presence of appreciable convective motion. The Dufour effect is even smaller. The terms in the energy equation (3) corresponding to viscous dissipation and the pressure field will later be ignored, since they are very small in such flows. In addition, they do not admit similarity in some of the circumstances of greatest practical importance, as we shall see later.

The x direction is first taken positive in the direction opposed to gravity, i.e. $\mathbf{g} = -g\mathbf{i}$, where $\mathbf{i}$ is a unit vector in the x direction, for upward buoyancy. The local static pressure p is written as the sum of the local motion pressure p_m and the hydrostatic pressure p_h in the remote ambient medium, where $dp_h/dx = -g\rho_\infty$ and ρ_∞ is the local ambient density (at x). We now have

$$\mathbf{F} - \nabla p = -g\rho\mathbf{i} + g\rho_\infty\mathbf{i} - \nabla p_m = g(\rho_\infty - \rho)\mathbf{i} - \nabla p_m. \tag{5}$$

The first term in (5) is the buoyancy force and in general $\rho_\infty = \rho(t_\infty, s_\infty, p_\infty)$. Now applying the boundary-layer approximations for two-dimensional plane flows largely in the x direction, we have

$$\partial u/\partial x + \partial v/\partial y = 0, \tag{6}$$

$$\rho_1\left(u\frac{\partial u}{\partial x} + v\frac{\partial u}{\partial y}\right) = \mu\frac{\partial^2 u}{\partial y^2} + g(\rho_\infty - \rho), \tag{7}$$

$$\rho_1 c_p\left(u\frac{\partial t}{\partial x} + v\frac{\partial t}{\partial y}\right) = k\frac{\partial^2 t}{\partial y^2} + \beta Tu\frac{dp_h}{dx} + \mu\left(\frac{\partial u}{\partial y}\right)^2, \tag{8}$$

$$u\frac{\partial s}{\partial x}+v\frac{\partial s}{\partial y} = D\frac{\partial^2 s}{\partial y^2}. \tag{9}$$

Following the notation of Gebhart (1971, 1973), we define a transformation in terms of a similarity variable $\eta(x,y)$ and stream functions $\psi(x,y)$ and $f(\eta)$ and also define the temperature and salinity functions:

$$\eta = yb(x), \quad \psi(x,y) = \nu c(x)f(\eta), \tag{10}$$

$$t_0-t_\infty = d(x), \quad s_0-s_\infty = e(x), \tag{11}$$

$$t_\infty-t_r = j(x), \quad s_\infty-s_r = r(x), \tag{12}$$

$$\phi = (t-t_\infty)/t_0-t_\infty, \quad S = (s-s_\infty)/(s_0-s_\infty), \tag{13}$$

where t_r and z_r are reference values and ν is also taken as constant, as was μ, since changes in ρ are very small. The density correlation (20) indicates that the density change is even very much smaller than in ordinary liquids. For example, the change $\Delta\rho$ from 0 to 5 °C is about 200 p.p.m. of ρ_m. The salinity variable used is that given in (13), instead of s/s_∞, for simplicity in subsequent analysis. The functions d and e concern the variables t and s at $y = 0$, while j and r admit stratification of the quiescent ambient medium. The functions b and c depend on the local vigour and extent of the flow.

The local vigour of a buoyancy-induced flow is indicated by the local Grashof number, which is conventionally defined as $Gr_x = g\beta x^3(t_0-t_\infty)/\nu^2$ for a purely thermally driven flow. This results from analysis with what is often called the second part of the Boussinesq approximation. The first part is that used in (1). The second amounts to assuming that density is a linear function of temperature. There are considerable differences and confusion in the literature concerning the proper attribution and names to be associated with these approximations. There is a widely used convention which calls them Boussinesq. However they were first introduced by Oberbeck (1879). They were also used by Lorenz (1881) in the pioneering boundary-region calculation of a buoyancy-induced flow, some twenty-one years before the specific enunciation of forced-flow boundary-layer theory. The discussion by Joseph (1971) suggests that these be called collectively the O–B approximations. We have here retained the more conventional term.

The above Grashof number is the 'unit Grashof number' gx^3/ν^2 times a measure $\beta(t_0-t_\infty)$ of the units of buoyancy. When additional buoyancy modes arise owing to species diffusion, additional units of buoyancy of similar form are added. See, for example, Gebhart & Pera (1971).

Around an extremum one may not estimate the buoyancy force with a single linear term. Some true measure of the motive density difference $\Delta\rho_G$ must be used as follows:

$$Gr_x = \frac{gx^3}{\nu^2}\frac{\Delta\rho_G}{\rho_2}. \tag{14}$$

We might take $\Delta\rho_G = \rho_\infty-\bar{\rho}$, where $\bar{\rho}$ is some suitable average value associated with the convection region. Simple averaging of the two boundary temperatures t_0 and t_∞ yields $\Delta\rho_G = \frac{1}{2}\rho\beta(t_0-t_\infty)$, using the conventional approximation. An analogous and more reasonable procedure here might be to calculate $\bar{\rho}$ as the average of $\rho(t,s,p)$ between both the bounding temperature and salinity conditions, assuming, as justified later, that the pressure effects are very commonly of smaller order.

However, this relatively simple measure was found not to be the proper one on two counts. First, with extrema, the boundary conditions are not always characteristic. Second, the Grashof number should be a measure of the strength of the flow and should generally indicate its direction. One may easily see, by locating different t_0 and t_∞ conditions on figure 1, that use of the average of these two conditions in $\Delta\rho_G$ does not in general confer any of these properties on the Grashof number. Instead it was found very advantageous to define $\Delta\rho_G$ as the actual calculated physical buoyancy force across the convection layer. This definition will be seen to arise naturally.

Introducing the transformations (10)–(13) into (6)–(9), we have

$$f''' + \frac{c_x}{b} f f'' - \left(\frac{c_x}{b} + \frac{cb_x}{b^2}\right) f'^2 + \frac{g}{\nu^2 cb^3} \frac{(\rho_\infty - \rho)}{\rho_1} = 0, \tag{15}$$

$$\frac{\phi''}{\sigma} + \frac{c_x}{b} f\phi' - \frac{cd_x}{bd} f'\phi - \frac{cj_x}{bd} f' - \beta T \frac{c}{bd} \frac{g}{c_p} f' + \frac{b^2c^2}{d} \frac{\nu^2}{c_p} f''^2 = 0, \tag{16}$$

$$\frac{S''}{Sc} + \frac{c_x}{b} fS' - \frac{ce_x}{be} f'S - \frac{cr_x}{be} f' = 0, \tag{17}$$

where the subscripts x indicate differentiation with respect to x. The last term in (15) is the buoyancy force.

Both (16) and (17) contain terms for non-uniform surface conditions, those in d_x and e_x, and also terms for stratification of the ambient medium, those in j_x and r_x. The energy effects of variations in the hydrostatic pressure and of viscous dissipation are retained in (16).

An analysis for conditions of similarity must await the specification of $\rho_\infty - \rho$. This is done in later sections, first for thermal buoyancy alone, then for combined buoyancy modes. Similarity will later be achieved for conditions of very broad practical importance.

With similarity, the apparent boundary conditions will be

$$1 - \phi(0) = 1 - S(0) = \phi(\infty) = S(\infty) = f'(0) = f'(\infty) = 0. \tag{18}$$

The other conditions result from considerations at $\eta = 0$. For a strictly impermeable surface

$$f(0) = S'(0) = 0. \tag{19}$$

However, this would admit no salt diffusion, except with saline stratification in the ambient medium. Other surface conditions might be considered, e.g. a melting or freezing ice surface or dissolving salt.

3. A density dependence

The above formulation carries us as far as we can go without specifying $\rho(t, s, p)$. The importance of the properties of saline water have led, over many years, to many investigations of the dependence of density on t, s and p. There are many tabulations of data and suggested equations of state. There has been a progressive improvement of accuracy and a broadening of the range of conditions covered.

Chen & Millero (1976) have presented a new density equation of state for water which is valid for pressures up to 1000 bars and salinities up to 40 p.p.t. This relation agrees with data to within the order of 10 p.p.m. However, it was not developed for accuracy in the region of inversion and contains some 35 temperature terms in very complicated combinations.

Therefore Gebhart & Mollendorf (1977) have developed a much simpler relation for $\rho(t,s,p)$ which is of comparable accuracy and yet of sufficient simplicity to yield fluid-motion formulations which admit many similarity solutions, with very few new parameters. This density equation of state, with a single temperature term, is

$$\rho(t,s,p) = \rho_m(s,p)\{1-\alpha(s,p)\,[|t-t_m(s,p)|]^{q(s,p)}\}, \tag{20}$$

where

$$\begin{aligned}\rho_m(s,p) &= \rho_m(0,1)\,[1+f_1(p)+sg_1(p)+s^2h_1(p)]\\ &= \rho_m(s_\infty,p)\left[1+\frac{(s_0-s_\infty)\,Sg_1(p)+(s_0-s_\infty)^2\,S[S+2s_\infty/(s_0-s_\infty)]\,h_1(p)}{1+f_1(p)+s_\infty g_1(p)+s_\infty^2\,h_1(p)}\right]\\ &= \rho_m(s_\infty,p)\,[1+A(s_0,s_\infty,p)\,S+A'(s_0,s_\infty,p)\,S(S+E)],\end{aligned} \tag{21}$$

$$\begin{aligned}\alpha(s,p) &= \alpha(0,1)\,[1+f_2(p)+sg_2(p)+s^2h_2(p)]\\ &= \alpha(s_\infty,p)\,[1+B(s_0,s_\infty,p)\,S+B'(s_0,s_\infty,p)\,S(S+E)],\end{aligned} \tag{22}$$

$$\begin{aligned}t_m(s,p) &= t_m(0,1)\,[1+f_3(p)+sg_3(p)+s^2h_3(p)]\\ &= t_m(s_\infty,p)\,[1+C(s_0,s_\infty,p)\,S+C'(s_0,s_\infty,p)\,S(S+E)],\end{aligned} \tag{23}$$

$$\begin{aligned}q(s,p) &= q(0,1)\,[1+f_4(p)+sg_4(p)+s^2h_4(p)]\\ &= q(s_\infty,p)\,[1+D(s_0,s_\infty,p)\,S+D'(s_0,s_\infty,p)\,S(S+E)].\end{aligned} \tag{24}$$

The $(0,1)$ quantities above are those for pure water at 1 bar abs. The f_i, g_i and h_i are polynomials in $p-1$; see the appendix. Some polynomials may be taken as zero in simpler, though less accurate, formulations. The above f_i are not to be confused with the generalized stream function f defined in (10).

We see that $\rho(t,s,p)$ is temperature dependent only as $|t-t_m|^q$. This form leads to extremely important simplifications of the flow analysis. For example, gradients in salinity are often much more important than those of pressure in wide ranges of applications. Thus, in the last forms of (21)–(24), the coefficients A, B, C, D, etc., are constants, with s_0 constant and without saline stratification, and (20) becomes very much simpler for analysis. This greatly reduces the number of additional parameters which will arise.

The $(0,1)$ quantities and the pressure polynomials f_i, g_i and h_i were determined by a nonlinear regression fit, with the smallest r.m.s. difference, to perhaps the best collection of information. This is the pure-water collection of Fine & Millero (1973) and the saline-water density data of Chen & Millero (1976). The range of the regression was t = 0–20 °C, s = 0–40 p.p.t. and p = 1–1000 bars. This range of conditions includes the vast majority of terrestrial surface water.

The most accurate form of (20) obtained was with third-order polynomials for f_i, g_i and h_i. The resulting r.m.s. fit was within 3·5 p.p.m. for pure water and within 10·4 p.p.m. for the 309 saline-water data points of Chen & Millero (1976) which fell in the chosen range of conditions. The resulting values of the parameters are tabulated in the appendix. We have also determined a much simpler form of (20) with $n = 2$, no s^2 terms and q independent of s; see the appendix. Even with these drastic simplifications, the r.m.s. differences are only 6·5 p.p.m. and 38·2 p.p.m. respectively. The

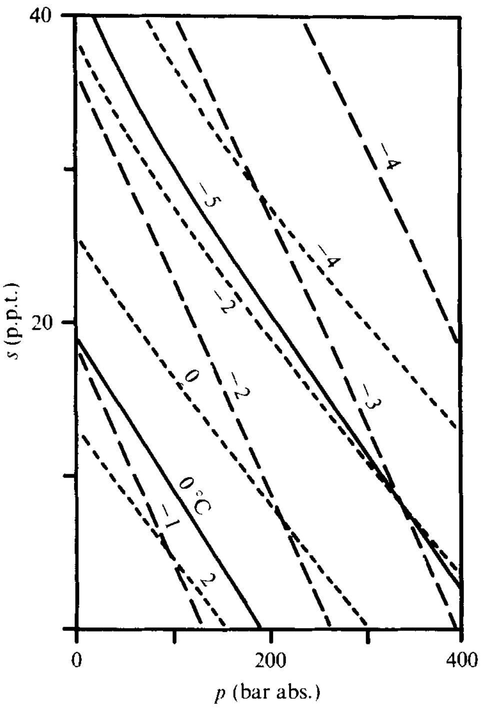

FIGURE 2. Variations of the temperature $t_m(s,p)$ from (23) at maximum density, the phase equilibrium temperature $t_{il}(s,p)$ from (25) and of their difference $t_m(s,p)-t_{il}(s,p)$ over a range of salinities and pressures. ——, $t_m(s,p)$; - - -, $t_{il}(s,p)$; - - - - - -, $t_m - t_{il}$. The numbers on the curves are in °C.

effects of salinity and pressure on ρ, ρ_m and t_m may be seen in figure 1. The variation of t_m with salinity and pressure, from our correlation (23), is shown as the solid curves in figure 2. The area corresponding to actual density measurements is that for temperatures of about 0 °C and above.

Note that the parameters of this correlation, like those in other equations of high accuracy, are determined to many digits. Retaining seven digits in the correlation leaves density unaffected by round-off to 0·1 p.p.m. over the whole range of conditions covered. This level is dictated by the expected precision level of the best past density information. It is also consistent with the needs for precision in analysis. For example, for pure water at 1 bar, the density change from t_m to $t_m + 0{\cdot}1$ °C is only 0·1 p.p.m. This small difference also demonstrates both the fundamental difficulty in determining t_m directly and the imprecision in the traditionally quoted values. These matters are discussed in detail by Gebhart & Mollendorf (1977).

It is interesting to compare the accuracy of the equally simple correlation

$$\rho = \rho_m[1 - 8 \times 10^{-6}(t - t_m)^2]$$

for pure water at 1 atm used in some past analyses with the result from (20). The r.m.s. difference at 2 °C intervals between 0 and 20 °C is 9·8 p.p.m. This is very significant, since a density difference of 100 p.p.m. from ρ_m corresponds to a temperature difference of about 3 °C on either side of t_m.

The temperature range of validity of the following analysis, for equilibrium phase changes, is bounded below by the equilibrium ice-melting temperature t_{il}. This was recently determined by Fujino, Lewis & Perkin (1974) to be

$$t_{il}(s,p) = -0{\cdot}02831 - 0{\cdot}0499s - 0{\cdot}000112s^2 - 0{\cdot}00759p \tag{25}$$

when corrected through personal communication with Dr E. L. Lewis and converted to bars absolute. The data range was 17·7 p.p.t. $\leqslant s \leqslant$ 35 p.p.t. and 1 atm $< p <$ 100 atm. This result is corroborated by the measurements by Doherty & Kester (1974). Contours of constant t_{il} *vs.* salinity and pressure are shown in figure 2 as dashed curves. Large depressions in the equilibrium melting temperature are seen at high salinities and pressures. It can be seen in figure 1 that t_m decreases more rapidly than t_{il} with increasing salinity and pressure.

Using (25) in conjunction with $t_m(s,p)$, we show the variation of $t_m - t_{il}$ with salinity and pressure in figure 2, also as dashed curves. The equilibrium limits for the occurrence of a density extremum are seen to be about $p <$ 300 bars in pure water and about $s <$ 25·5 p.p.t. at a pressure of 1 bar. However, we recall that, in freezing ice from pure water and possibly also from saline water, substantial temperature depressions below the equilibrium condition (25) often occur and may persist for long periods. There is some indication that our density correlation also applies accurately in this subcooling range. In particular, our inferred value of $t_m(0,p)$, even at high pressures, agrees well with new direct measurements by Caldwell (1977) in such subcooled pure water. However, there is no way to check this density prediction directly, since modern density data have been determined at about 0 °C and above.

4. Analysis, for thermal buoyancy effects alone

Consider first vertical flows of small extent, compared with any vertical salinity gradient, in an extensive and quiescent ambient medium. For simplicity we shall first treat a flow generated by conditions which do not also result in mass diffusion. This would occur, for example, with vertical heated or cooled impermeable surfaces in either pure or saline water. The results may also be applied, with some small additional approximation, to a vertical surface of ice formation or melting in pure water. Thus $s = s_\infty$ and $\rho(t,s,p) = \rho(t,s_\infty,p)$ or $\rho(t,0,p)$ in pure water.

A simplification is found, for all flows, for the motion-pressure effect on the density difference $\rho_\infty - \rho$. The approximations which resulted in (7) include the omission of the motion pressure p_m. Specifically, the largest term in p_m $(\partial p_m/\partial y)$ may be neglected for any fluid of ordinary Prandtl number. The motion-pressure difference Δp_m across the flow region is very much less than $gL\Delta\rho_G$, where L is the characteristic vertical dimension. In a liquid this is also negligible compared with the hydrostatic difference $\Delta p_h = gL\rho_\infty$.

The hydrostatic variation itself may also be seen, from the values in the appendix, to have a very small effect on the density even for a flow of great vertical extent. For example, we see from (21) that the leading pressure effect on the density level, from table 6 (see appendix), is about $5\times 10^{-6}L\,(\mathrm{m})$ compared with 1·0. Another way of estimating this is to compare the leading salinity and pressure terms. Their ratio $6\times 10^{-3}L/s$ (p.p.t.) shows that an uncertainty of 1 p.p.t. is equivalent to $L = 160\,\mathrm{m}$.

Condition	t_0	t_∞	R	Net buoyancy force
Heating water, $t_0 > t_\infty$	$\frac{1}{2}t_m$	0	2	Down
	t_m	0	1	Down
	$2t_m$	0	$\frac{1}{2}$	Down
	$3t_m$	0	$\frac{1}{3}$	Down
	$4t_m$	0	$\frac{1}{4}$	Up
	$2t_m$	t_m	0	Up
	$3t_m$	$2t_m$	-1	Up
	$4t_m$	$3t_m$	-2	Up
	$10t_m$	$9t_m$	-8	Up
Melting or freezing of ice at 1 bar, or cooling of water, $t_0 < t_\infty$	0	$\frac{1}{2}t_m$	-1	Up
	0	t_m	0	Up
	0	$\frac{3}{2}t_m$	$\frac{1}{3}$	Down
	0	$2t_m$	$\frac{1}{2}$	Down
	0	$4t_m$	$\frac{3}{4}$	Down
	$\frac{1}{2}t_m$	t_m	0	Up
	$\frac{1}{2}t_m$	$\frac{5}{4}t_m$	$\frac{1}{3}$	Down
	$\frac{1}{2}t_m$	$2t_m$	$-\frac{2}{3}$	Down
	t_m	$2t_m$	1	Down
	$8t_m$	$9t_m$	8	Down

TABLE 1. Some transport conditions, values of R and buoyancy directions.

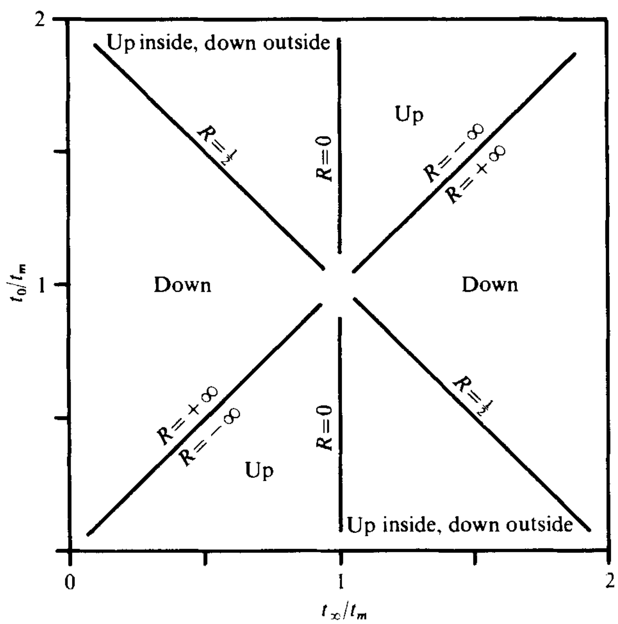

FIGURE 3. The direction of the buoyancy force W, which is determined by the values of t_0, t_∞, t_m and, therefore, of R.

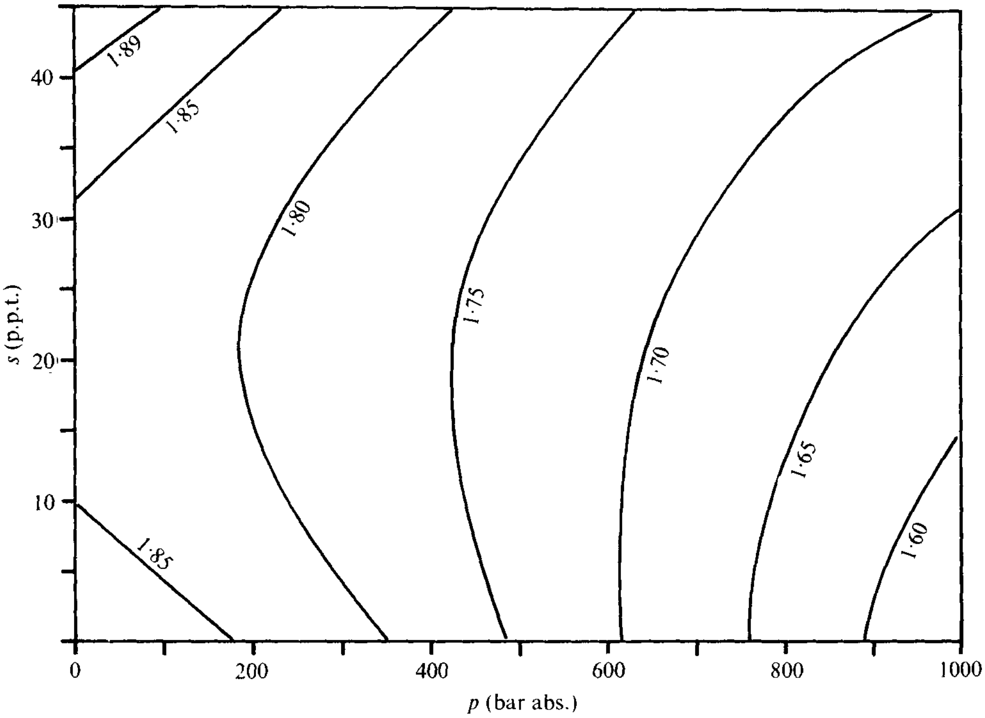

FIGURE 4. Variation of the exponent $q(s,p)$ with salinity and pressure from the correlation of Gebhart & Mollendorf (1977) for $P = 48$ and $n = 3$.

Therefore we shall neglect pressure effects on density throughout any particular flow region. The pressure terms in (20) then pertain only to the pressure level. The density difference is then

$$\begin{aligned}\rho_\infty - \rho &= \rho(t_\infty, s_\infty, p) - \rho(t, s_\infty, p) = \rho_m(s_\infty, p)\,\alpha(s_\infty, p)\,[|t-t_m|^q - |t_\infty - t_m|^q] \\ &= \rho_m \alpha[|t-t_m|^q - |t_\infty - t_m|^q], \qquad (26a)\end{aligned}$$

where $t_m = t_m(s_\infty, p)$. Both temperature terms are always taken positive, since ρ_m is a maximum. If we define

$$R = \frac{t_m(s_\infty, p) - t_\infty}{t_0 - t_\infty}, \qquad (26b)$$

the density difference becomes

$$\rho_\infty - \rho = \rho_m \alpha |t_0 - t_\infty|^q [|\phi - R|^q - |R|^q] = \rho_m \alpha |t_0 - t_\infty|^q W. \qquad (26c)$$

The new parameter R indicates the relation between t_0, t_∞ and the extremum temperature and, as a result, determines the distribution and direction of the buoyancy force W across the flow region. For example, for $t_\infty = t_m$, i.e. $R = 0$, the buoyancy force is always upward. However, for $t_0 = t_m$, i.e. $R = 1$, it is always downward. There may also be buoyancy reversals. For example, taking $t_0 = 0\,^\circ\mathrm{C}$ and $t_\infty = \frac{3}{2}t_m(^\circ\mathrm{C})$ gives $R = \frac{1}{3}$. The buoyancy force is upward very near the surface and downward otherwise. Large values of R result for both t_0 and t_∞ well away from t_m. Table 1 and figure 3 indicate some of the many possibilities. Most past analyses of vertical flows have been, in effect, for $q = 2$ and $R = 0$ in the present formulation. This results in $W = \phi^2$ in

(26*c*). In (20), q ranges between about 1·9 and 1·6, depending on the salinity and pressure. Contours of constant q were determined, to three significant digits, from the roots of (24). The results are shown in figure 4 for a range of salinities and pressures.

Similarity

A sufficient condition for similarity is that the following quantities in (15), (16) and (26*b*) be independent of x:

$$C_1 = \frac{c_x}{b}, \quad C_2 = \frac{cb_x}{b^2}, \quad C_3 W = \frac{g\alpha\rho_m|t_0-t_\infty|^q W}{\rho_1 \nu^2 c b^3}. \tag{27}$$

Clearly we should choose $\rho_m(s,p) = \rho_1$. Here the subscripts x mean differentiation with respect to x.

We see from (26*c*) that if $\phi = \phi(\eta)$, as is also necessary in (16), then W is independent of x only if R is. A sufficient condition for this is $R = 0$, i.e. $t_\infty = t_m$ with the ambient medium at the extremum density ρ_m (s_∞, p). This is the case treated by Goren (1966), Govindarajulu (1970), Roy (1972) and Soundalgekar (1973), but with $s_\infty = 0$ and $q = 2$. Otherwise, we must have $t_0 - t_\infty = d \propto (t_m - t_\infty) \propto j$. Setting temperature stratification aside for the moment, the requirement is that both t_0 and t_∞ be independent of x. Then R need not be zero.

From C_1 and C_2 it may be shown that both b and c are either power-law or exponentially dependent on x. We choose $C_1 = 3$, $C_3 = 1$ and $C_2 = -1$ for $n = 0$. This results in

$$b(x) = \frac{1}{x}\left(\frac{g\alpha x^3 d^q}{4\nu^2}\right)^{\frac{1}{4}} = \frac{c(x)}{4x}. \tag{28}$$

This suggests that the Grashof number be defined as follows:

$$Gr'_x = g\alpha(s_\infty, p)\, x^3 |t_0 - t_\infty|^q / \nu^2. \tag{29}$$

However, we note that this quantity is always positive, even though the buoyancy force W may be either positive or negative, depending on the values of t_0 and t_∞ relative to t_m. This deficiency may be removed by using instead a form of Gr_x dependent on $\Delta\rho_G$ as in (14). We take $\Delta\rho_G$ as the integral of the buoyancy difference $\rho_\infty - \rho$ across the convection layer. This amounts to integrating W (over η); see (26*c*). The integral is defined as

$$I_w = \int_0^\infty W d\eta = \int_0^\infty [|\phi - R|^q - |R|^q]\, d\eta \tag{30}$$

and the Grashof number becomes

$$Gr_x = g\alpha(s_\infty, p)\, x^3 |t_0 - t_\infty|^q I_w / \nu^2. \tag{31}$$

When this value of Gr_x is used in (28), instead of (29), the buoyancy-force term in (15) becomes

$$F(\eta) = W / I_w. \tag{32}$$

Thus $I_w < 0$ will often signal a need, in (31), to reinterpret x as positive in the direction of $\mathbf{g}$. Then $F(\eta)$ would be, on the average, positive across the flow region. This question is that of 'convective inversion' and will be clarified later. Additional considerations in the normalization of W by I_w are that we then always deal with a buoyancy-force term of order one over most of the region. On the other hand, we are now faced with integro-differential equations since we must also iterate on I_w in the numerical scheme.

Other similar solutions

Additional conditions under which similarity solutions exist will be set forth here before discussing calculations. Recall that, in addition to $R = 0$, i.e. $t_\infty = t_m$, the condition $t_0 - t_\infty = d(x) \propto t_m - t_\infty = (t_m - t_r) - (t_\infty - t_r) = t_m - t_r - j(x)$ also results in $W = W(\eta, R)$ for $\phi = \phi(\eta)$. In addition, from (16)

$$cd_x/bd = C_5 \tag{33}$$

must be independent of x. This arises from the x dependence of $t_0 - t_\infty$ and is satisfied by

$$d(x) = t_0 - t_\infty = Nx^n, \quad C_5 = 4n.$$

With this variation, Gr_x, b and c are unchanged. However, the constants now become $C_1 = qn + 3$, $C_2 = qn - 1$ and $C_3 = 1$. Admitting temperature stratification requires that

$$cj_x/bd = C_7 \tag{34}$$

must be independent of x, which implies that $j(x) = (t_\infty - t_r) = (C_7 N/4n)\, x^n$ and $C_7 = 4nN_\infty/N$. If $R = 0$, i.e. $t_\infty = t_m$, we may not have stratification since

$$t_m = t_m(s_\infty, p) = \text{constant}.$$

If $R \neq 0$, then

$$R = (t_m - t_r - N_\infty x^n)/Nx^n$$

is independent of x only for t_m chosen as t_r. Then $R = -N_\infty/N$.

The ambient medium will be quiescent only for stable stratification. The condition for this in the absence of mass diffusion is $j_x \geqslant -g(\partial T/\partial p)_S$, where S is the entropy. Since $(\partial T/\partial p)_S$ is positive and small for most states of liquids, the more conservative and convenient condition $j_x \geqslant 0$ is often taken; see Gebhart (1973). However, in fact $(\partial T/\partial p)_S = \beta T/\rho c_p$ and the exact condition is

$$j_x = Nnx^{n-1} \geqslant -\frac{g\beta T}{c_p}, \quad \beta = -\frac{1}{\rho}\left(\frac{\partial \rho}{\partial T}\right)_p. \tag{35}$$

Noting that g, T and c_p are positive, the sign of the limit is determined by that of β, which is negative below t_m. Thus the stable limit allows decreasing t_∞ for $t_\infty > t_m$ but increasing t_∞ is required for $t_\infty < t_m$.

Considering now the viscous dissipation mode of thermal energy production in (16), we find

$$\frac{b^2c^2}{d}\frac{\nu^2}{c_p} = C_6 = \frac{4g\alpha N^{q-1}}{c_p}\, x^{n(q-1)+1}. \tag{36}$$

This effect is of order $4g\alpha NPrL^{n(q-1)+1}/c_p$ compared with conduction, for example. Similarity results only for $n = -1/(q-1)$, which is an unrealistic circumstance. We note that this effect, dependent on $g\alpha$, is very small. Now the pressure term in (16) is rewritten as

$$C_{10} = \frac{gT}{c_p}\frac{c}{bd}\beta = \frac{gT}{c_p}\frac{c}{bd}\frac{\alpha q|\phi - R|^{q-1}|t_0 - t_\infty|^{q-1}}{1 - \alpha|\phi - R|^q|t_0 - t_\infty|^q}\frac{(\phi - R)\,(t_0 - t_\infty)}{|\phi - R|\;|t_0 - t_\infty|}, \tag{37a}$$

where β is evaluated from (20) and the last quantity assures the proper sign when β is not zero. Neglecting the second term in the denominator compared with one, we have

$$C_{10} = (4Tg\alpha q/c_p)\,|\phi - R|^{q-2}(\phi - R)|N|^{q-2}x^{1-n(2-q)}. \tag{37b}$$

This is similar for $n = \frac{1}{2}(2-q)$, quite a large value, if one neglects the variation of T across the flow field. This term also depends on $g\alpha$ and is very small.

Equations (15) and (16), neglecting these last two effects and taking $t_r = t_m$ if stratification is present, are then

$$f''' + (3+qn)ff'' - (2+2qn)f'^2 + F = 0, \tag{38a}$$

$$\phi'' + \sigma[(3+qn)f\phi' - 4nf'\phi - (4nN_\infty/N)f'] = 0 \tag{38b}$$

for Gr_x and buoyancy defined as in (31) and (32). If Gr_x is defined as in (29) then F in (38a) is replaced by W. We shall use the form (31) and $F = W/I_w$ exclusively hereafter. For an impermeable surface we have

$$1 - \phi(0) = \phi(\infty) = f'(0) = f(0) = f'(\infty) = 0. \tag{39}$$

This formulation supposes that x increases in the direction of the net flow. Uncertainties arise in the range $0 < R < \frac{1}{2}$. There $W(\eta)$ is small and changes sign. The net flow direction may, perhaps, be determined by the sign of I_w. Using Gr_x as defined with I_w in (31), we find the $+x$ direction. Normalizing the buoyancy force with I_w enhances its magnitude.

Other conditions

Here we develop additional limits on the reasonableness of solutions, as well as the basic transport relations. The local surface heat flux $q''(x)$, the energy $Q(x)$ convected locally by the flow, the local flow-region thickness $\delta(x)$ and the local Nusselt number Nu_x are

$$q''(x) = -k(\partial t/\partial y)_0 = [-\phi'(0)]\,kdb \propto x^{\frac{1}{4}[n(q+4)-1]}, \tag{40}$$

$$Q''(x) = \int_0^\infty \rho c_p(t - t_\infty)\,u\,dy = \rho c_p \nu c d \int_0^\infty \phi f' d\eta \propto x^{\frac{1}{4}[n(q+4)+3]}, \tag{41}$$

$$\delta(x) = \eta_\delta/b \propto x^{\frac{1}{4}(1-nq)}, \tag{42}$$

$$Nu_x = \frac{h_x x}{k} = \frac{q''(x)}{d}\frac{x}{k} = [-\phi'(0)]\frac{G}{4} = \frac{-\phi'(0)}{2^{\frac{1}{2}}}Gr_x^{\frac{1}{4}}. \tag{43}$$

The requirement that $\delta(0) = 0$ results in $nq < 1$, or $n < 0{\cdot}528$ at 1 bar abs. in pure water. With the $+x$ direction taken such that f' is essentially positive, $Q(x)$ must, for $N > 0$, be a constant, a line source at $x = 0$ or increase with x. Thus

$$n \geqslant -3/(q+4) = -0{\cdot}509.$$

The limits are then $-0{\cdot}509 \leqslant n < 0{\cdot}528$. The comparable result for the usual buoyancy-force approximation is $-0{\cdot}6 \leqslant n < 1$. The lower limits in both analyses are the plane plume or an adiabatic surface with a horizontal line source at the leading edge. The condition of a uniform surface heat flux is here $n = 1/(4+q) = 0{\cdot}1697$. The Nusselt number is the same as before, except for the definition of Gr_x. Also, the value of $\phi'(0)$ depends on Pr, R and the buoyancy formulation embodied in (38a).

(a)

R	$\sigma = 8{\cdot}6$	$\sigma = 9{\cdot}6$	$\sigma = 10{\cdot}6$	$\sigma = 11{\cdot}6$	$\sigma = 12{\cdot}6$	$\sigma = 13{\cdot}6$
−16·00	0·81163, 1·37935	0·82000, 1·43954	0·82729, 1·49562	0·83370, 1·54822	0·83941, 1·59783	0·84453, 1·64484
	9·97224, 0·31966	9·54472, 0·31352	9·17826, 0·30813	8·85929, 0·30334	8·57825, 0·29903	8·32796, 0·29512
−14·00	0·81178, 1·37920	0·82015, 1·43938	0·82743, 1·49545	0·83384, 1·54804	0·83954, 1·59764	0·84466, 1·64465
	8·87115, 0·31957	8·49086, 0·31343	8·16489, 0·30804	7·88115, 0·30325	7·63116, 0·29894	7·40852, 0·29503
−12·00	0·81198, 1·37900	0·82034, 1·43917	0·82761, 1·49523	0·83402, 1·54781	0·83971, 1·59740	0·84483, 1·64439
	7·75370, 0·31944	7·42135, 0·31330	7·13646, 0·30792	6·88848, 0·30313	6·67000, 0·29882	6·47541, 0·29491
−10·00	0·81226, 1·37872	0·82061, 1·43887	0·82787, 1·49491	0·83427, 1·54748	0·83995, 1·59705	0·84507, 1·64403
	6·61691, 0·31927	6·33332, 0·31313	6·09022, 0·30775	5·87863, 0·30296	5·69220, 0·29865	5·52615, 0·29475
−8·00	0·81267, 1·37830	0·82100, 1·43843	0·82825, 1·49445	0·83463, 1·54699	0·84031, 1·59654	0·84541, 1·64350
	5·45652, 0·31900	5·22271, 0·31287	5·02228, 0·30749	4·84782, 0·30271	4·69411, 0·29841	4·55720, 0·29451
−4·00	0·81463, 1·37631	0·82289, 1·43631	0·83007, 1·49221	0·83640, 1·54465	0·84203, 1·59410	0·84708, 1·64095
	3·03451, 0·31774	2·90460, 0·31164	2·79323, 0·30628	2·69629, 0·30151	2·61086, 0·29723	2·53478, 0·29334
−3·00	0·81586, 1·37506	0·82408, 1·43498	0·83122, 1·49081	0·83751, 1·54317	0·84311, 1·59256	0·84813, 1·63935
	2·39704, 0·31694	2·29448, 0·31085	2·20656, 0·30551	2·13002, 0·30075	2·06257, 0·29648	2·00250, 0·29260
−2·00	0·81816, 1·37271	0·82629, 1·43249	0·83336, 1·48817	0·83959, 1·54041	0·84513, 1·58967	0·85010, 1·63635
	1·73858, 0·31544	1·66427, 0·30938	1·60056, 0·30406	1·54510, 0·29932	1·49623, 0·29507	1·45269, 0·29121
−1·00	0·82401, 1·36671	0·83193, 1·42611	0·83881, 1·48145	0·84487, 1·53335	0·85025, 1·58230	0·85508, 1·62868
	1·04801, 0·31154	1·00335, 0·30555	0·96504, 0·30030	0·93169, 0·29562	0·90230, 0·29142	0·87611, 0·28761
−0·50	0·83246, 1·35796	0·84007, 1·41681	0·84668, 1·47163	0·85249, 1·52305	0·85764, 1·57154	0·86227, 1·61749
	0·68233, 0·30570	0·65337, 0·29982	0·62853, 0·29467	0·60689, 0·29008	0·58782, 0·28596	0·57082, 0·28222
0·00	0·87166, 1·31584	0·87783, 1·37208	0·88316, 1·42445	0·88783, 1·47356	0·89195, 1·51986	0·89565, 1·56373
	0·28580, 0·27428	0·27393, 0·26910	0·26373, 0·26453	0·25483, 0·26046	0·24698, 0·25679	0·23998, 0·25346
0·50	0·71229, 1·47324	0·72425, 1·53934	0·73473, 1·60095	0·74401, 1·65875	0·75231, 1·71328	0·75978, 1·76494
	−0·16625, 0·37248	−0·15885, 0·36542	−0·15251, 0·35923	−0·14702, 0·35372	−0·14219, 0·34877	−0·13790, 0·34427
1·00	0·78491 1·40612	0·79426 1·46799	0·80241, 1·52564	0·80959, 1·57971	0·81600, 1·63072	0·82176, 1·67905
	−0·57804, 0·33574	−0·55296, 0·32930	−0·53149, 0·32366	−0·51281, 0·31864	−0·49637, 0·31412	−0·48173, 0·31003
2·00	0·80019, 1·39087	0·80898, 1·45178	0·81663, 1·50854	0·82338, 1·56177	0·82939, 1·61199	0·83478, 1·65957
	−1·30412, 0·32677	−1·24791, 0·32050	−1·19976, 0·31499	−1·15786, 0·31010	−1·12095, 0·30570	−1·08809, 0·30171
3·00	0·80405, 1·38700	0·81270, 1·44767	0·82022, 1·50420	0·82686, 1·55722	0·83276, 1·60723	0·83807, 1·65462
	−1·98107, 0·32442	−1·89585, 0·31819	−1·82281, 0·31272	−1·75926, 0·30786	−1·70327, 0·30348	−1·65342, 0·29952
4·00	0·80581, 1·38523	0·81440, 1·44579	0·82187, 1·50221	0·82845, 1·55514	0·83431, 1·60505	0·83957, 1·65235
	−2·63105, 0·32333	−2·51795, 0·31711	−2·42103, 0·31166	−2·33668, 0·30682	−2·26237, 0·30246	−2·19620, 0·29851
8·00	0·80828, 1·38274	0·81677, 1·44314	0·82416, 1·49942	0·83068, 1·55221	0·83647, 1·60200	0·84168, 1·64917
	−5·08154, 0·32179	−4·86335, 0·31560	−4·67634, 0·31018	−4·51359, 0·30535	−4·37021, 0·30102	−4·24252, 0·29708

TABLE 2 (*cont.*)

R	$\sigma = 8·6$	$\sigma = 9·6$	$\sigma = 10·6$	$\sigma = 11·6$	$\sigma = 12·6$	$\sigma = 13·6$
10·00	0·80875, 1·38227	0·81723, 1·44264	0·82460, 1·49889	0·83110, 1·55165	0·83688, 1·60141	0·84208, 1·64857
	−6·25063, 0·32149	−5·98230, 0·31531	−5·75232, 0·30989	−5·55216, 0·30507	−5·37582, 0·30074	−5·21878, 0·29681
12·00	0·80906, 1·38195	0·81753, 1·44231	0·82489, 1·49854	0·83138, 1·55128	0·83715, 1·60103	0·84234, 1·64817
	−7·39439, 0·32130	−7·07701, 0·31512	−6·80498, 0·30970	−6·56822, 0·30489	−6·35963, 0·30056	−6·17388, 0·29663
14·00	0·80928, 1·38173	0·81774, 1·44207	0·82509, 1·49829	0·83158, 1·55102	0·83735, 1·60076	0·84253, 1·64789
	−8·51762, 0·32116	−8·15207, 0·31499	−7·83874, 0·30957	−7·56605, 0·30476	−7·32579, 0·30043	−7·11183, 0·29650
16·00	0·80944, 1·38157	0·81789, 1·44190	0·82525, 1·49811	0·83172, 1·55083	0·83749, 1·60056	0·84267, 1·64767
	−9·62365, 0·32105	−9·21065, 0·31489	−8·85667, 0·30947	−8·54858, 0·30466	−8·27715, 0·30033	−8·03542, 0·29641

(*b*)

−16·00	0·83366, 1·54827, 7·88200, 0·30336	0·83352, 1·54846, 5·05622, 0·30346	0·33336, 1·54867, 3·09809, 0·30356
−14·00	0·83379, 1·54810, 7·04406, 0·30328	0·83363, 1·54832, 4·59765, 0·30339	0·83345, 1·54855, 2·87072, 0·30351
−12·00	0·83396, 1·54787, 6·18946, 0·30316	0·83377, 1·54813, 4·12118, 0·30329	0·83357, 1·54840, 2·62965, 0·30343
−10·00	0·83420, 1·54756, 5·31507, 0·30300	0·83397, 1·54786, 3·62302, 0·30315	0·83373, 1·54819, 2·37158, 0·30332
−8·00	0·83456, 1·54709, 4·41639, 0·30276	0·83427, 1·54746, 3·09758, 0·30295	0·83397, 1·54787, 2·09160, 0·30316
−4·00	0·83626, 1·54484, 2·51351, 0·30161	0·83571, 1·54558, 1·92274, 0·30198	0·83511, 1·54637, 1·42694, 0·30238
−3·00	0·83732, 1·54343, 2·00404, 0·30088	0·83661, 1·54439, 1·58733, 0·30137	0·83583, 1·54543, 1·22355, 0·30189
−2·00	0·83932, 1·54078, 1·47204, 0·29951	0·83829, 1·54218, 1·22242, 0·30021	0·83718, 1·54368, 0·99214, 0·30098
−1·00	0·84438, 1·53403, 0·90515, 0·29596	0·84257, 1·53656, 0·80930, 0·29723	0·84060, 1·53926, 0·71216, 0·29861
−0·50	0·85171, 1·52419, 0·59914, 0·29065	0·84878, 1·52841, 0·56943, 0·29277	0·84559, 1·53288, 0·53607, 0·29505
0·00	0·88641, 1·47642, 0·25798, 0·26169	0·88070, 1·48733, 0·27076, 0·26655	0·87372, 1·49943, 0·28657, 0·27236
0·50	0·74437, 1·65907, −0·14946, 0·35349	0·74573, 1·66027, −0·15872, 0·35261	0·74731, 1·66167, −0·16870, 0·35161
1·00	0·81033, 1·57891, −0·50907, 0·31818	0·81323, 1·57569, −0·49427, 0·31638	0·81658, 1·57177, −0·47673, 0·31430
2·00	0·82373, 1·56133, −1·11550, 0·30987	0·82507, 1·55965, −0·96627, 0·30901	0·82655, 1·55776, −0·82127, 0·30805
3·00	0·82708, 1·55694, −1·66760, 0·30771	0·82794, 1·55584, −1·35859, 0·30715	0·82887, 1·55463, −1·07990, 0·30654
4·00	0·82861, 1·55492, −2·19052, 0·30671	0·82924, 1·55411, −1·71146, 0·30630	0·82993, 1·55322, −1·29973, 0·30585
8·00	0·83076, 1·55210, −4·12344, 0·30530	0·83106, 1·55171, −2·92285, 0·30510	0·83139, 1·55128, −1·99646, 0·30488
10·00	0·83116, 1·55157, −5·03117, 0·30503	0·83140, 1·55125, −3·45863, 0·30487	0·83167, 1·55091, −2·28491, 0·30470
12·00	0·83143, 1·55121, −5·91274, 0·30485	0·83163, 1·55095, −3·96478, 0·30472	0·83185, 1·55067, −2·54933, 0·30457
14·00	0·83162, 1·55096, −6·77326, 0·30473	0·83179, 1·55074, −4·44769, 0·30461	0·83198, 1·55050, −2·79541, 0·30449
16·00	0·83176, 1·55078, −7·61624, 0·30463	0·83191, 1·55058, −4·91163, 0·30453	0·83207, 1·55037, −3·02686, 0·30443

TABLE 2. Heat-transfer and flow parameters for vertical flow without salinity gradients or local buoyancy reversals.

(*a*) $\left.\begin{matrix} f''(0), -\phi'(0) \\ I_w, f(\infty) \end{matrix}\right\}$ for $q(s, p) = q(0, 1) = 1·894816$.

(*b*) $f''(0)$, $-\phi'(0)$ I_w, $f(\infty)$ for $\sigma = 11·6$.

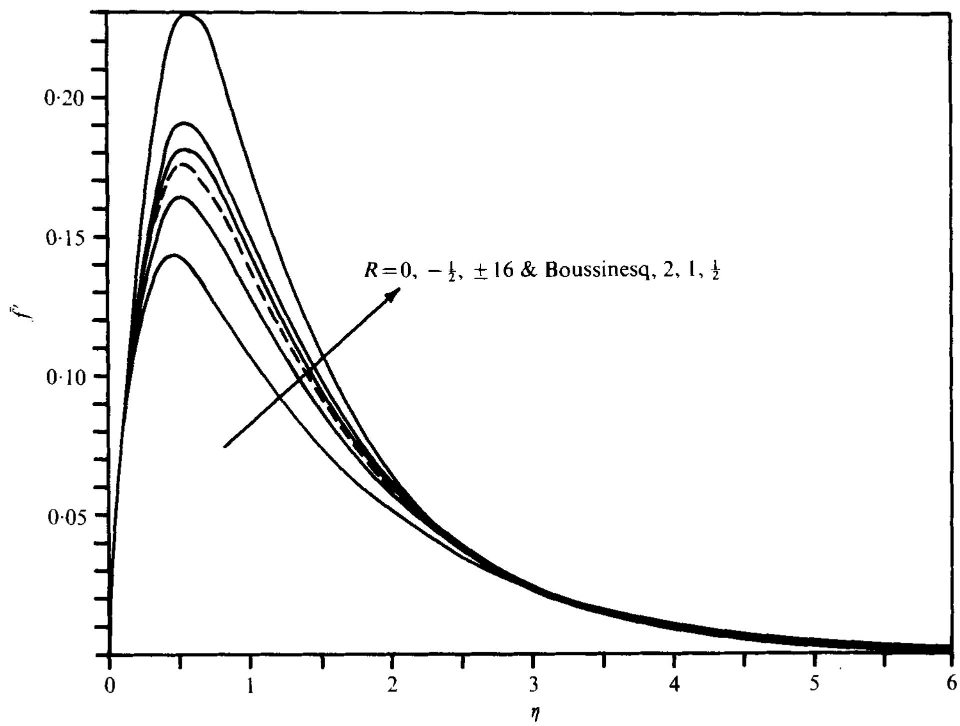

FIGURE 5. Calculated distribution of the velocity component parallel to the vertical surface for selected values of R, $\sigma = 11{\cdot}6$ and $q(s,p) = q(0,1) = 1{\cdot}894816$.

5. Numerical calculations for pure water

We first investigated the detailed transport predicted by (38) and (39), taking a Prandtl number σ of 11·6, that of pure water at 4 °C, and $q(s,p) = q(0,1) = 1{\cdot}894816$. We have retained for the calculations the full value of q for accuracy. Rounding q to 1·90 produces about a 2 % error in the units of buoyancy for $t_0 = 15$ °C and $t_\infty = 4$ °C. After discussing the results of the calculations we shall estimate the effect on overall transport parameters of rounding q.

Both t_0 and t_∞ were taken independent of x. The applications of such results are to the heating and cooling of water at temperatures around the inversion. However, we see from (38) that the flow and transport characteristics are entirely dependent on σ, q and R, since F depends only on these parameters.

In table 1 and figure 3 the value of R is related to temperature conditions and to the corresponding direction of the buoyancy force. Although the relation appears complicated at first, we see that the buoyancy force changes sign across the flow region only in the range $0 < R < \frac{1}{2}$. This is apparent in comparing cases in table 1 with the density distributions in figure 1. This is in accord with past observations with ice spheres in water. Dumoré *et al.* (1953) found 'convective inversion' at $t_\infty = 4{\cdot}8$ °C while Schenk & Schenkels (1968) estimated 5·3 °C. These temperatures correspond to $R = 0{\cdot}17$ and 0·25, respectively. These inversions were thought to be a complete flow reversal, which was accompanied by a drastic drop in transport, i.e. in the ice melting

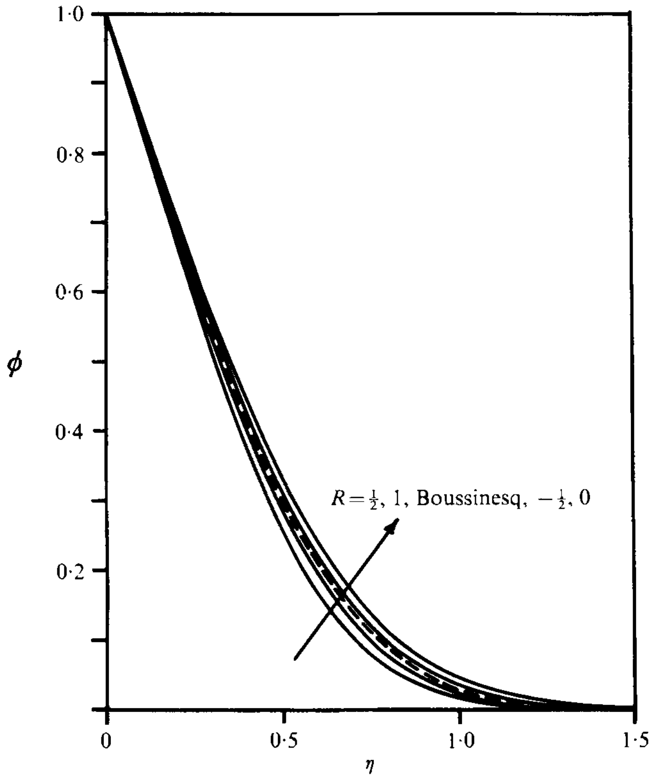

FIGURE 6. Calculated temperature distribution adjacent to vertical surface for selected values of R, $\sigma = 11{\cdot}6$ and $q(s,p) = q(0,1) = 1{\cdot}894816$.

rate. Bendell & Gebhart (1976) found that actual convective inversion occurred between 5·5 and 5·6 °C for flow adjacent to a vertical ice surface. Taking

$$t_m(0,1) = 4{\cdot}03\,^{\circ}\mathrm{C},$$

the resulting value of R is about 0·27.

On the other hand, $R \leqslant 0$ invariably gives upflow and $R \geqslant \frac{1}{2}$ invariably gives downflow, independent of heating or cooling. We note that R is negative only if t_∞ lies between t_0 and t_m. We also note that the linear approximation to $\rho_\infty - \rho$ will be approached at both large positive and large negative values of R, i.e. for

$$|t_0 - t_\infty| \ll |t_m - t_\infty|,$$

and equivalently for $q = 1$ and $R = 0$.

We initially investigated this R spectrum, first outside the buoyancy-reversal region, for $R = 0$, $\pm\frac{1}{2}$, ± 1, ± 2, ± 3, ± 4, ± 8, ± 10, ± 12, ± 14 and ± 16. For these values of R, calculations were performed for $q(s,p) = q(0,1) = 1{\cdot}894816$ and Prandtl numbers $\sigma = 8{\cdot}6$, 9·6, 10·6, 11·6, 12·6 and 13·6. Then for a single Prandtl number, $\sigma = 11{\cdot}6$, the effect of q variation was determined for $q(s,p) = q(0,100) = 1{\cdot}859663$, $q(0{,}500) = 1{\cdot}727147$ and $q(0{,}1000) = 1{\cdot}582950$ for the same values of R. These values of q also apply to saline water, e.g. $q(0,500) \approx q(40{,}600)$; see figure 4.

Accurate calculations in the region of net buoyancy-force reversal, i.e. $0 < R < \frac{1}{2}$,

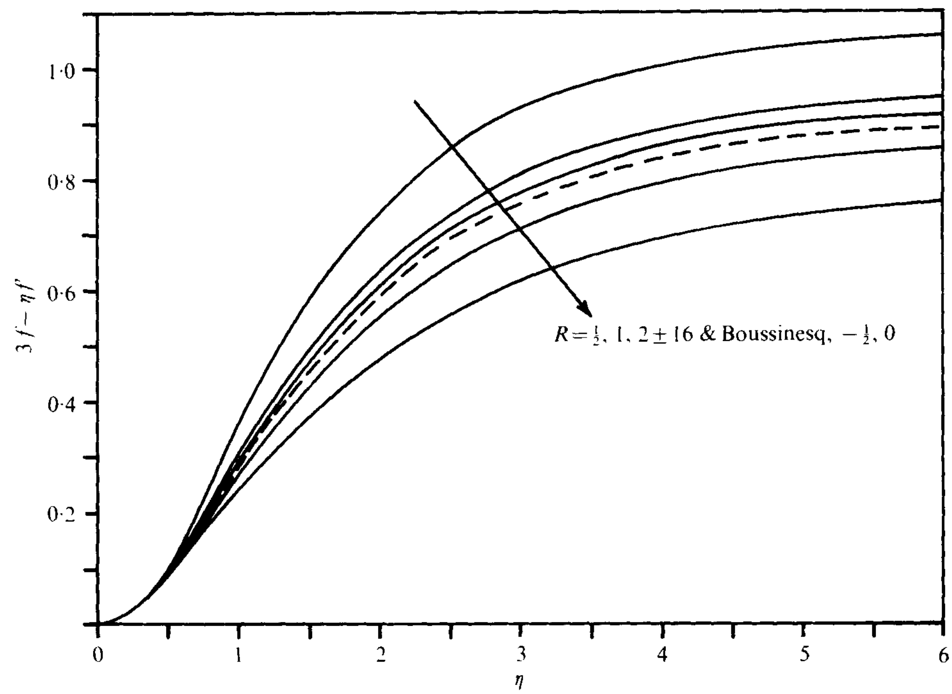

FIGURE 7. Calculated distribution of the velocity component normal to the vertical surface for selected values of R, $\sigma = 11{\cdot}6$ and $q(s,p) = q(0,1) = 1{\cdot}894816$.

proved to be unattainable. Local buoyancy-force reversal made numerical convergence extremely slow. Recall that convective inversion occurs in this range. Serious questions regarding the appropriateness of boundary-layer simplifications arise under such conditions. On the other hand, extrapolations of our results into this region agree very well with those of the heat-transfer measurements of Bendell & Gebhart (1976) which fall there.

Equations (38) were solved numerically subject to boundary conditions (39) for $n = N_x = 0$ and for the above ranges of σ, q and R. A predictor–corrector scheme, with automatic local subdivision of η to maintain prescribed accuracy, was used to integrate from $\eta = 0$ to $\eta = \eta_{\text{edge}}$. Initially unknown values of $\phi'(0)$, $f''(0)$ and I_w were guessed and subsequently corrected such that the far boundary conditions were satisfied. After investigating the effect of η_{edge}, $\Delta\eta$ and the accuracy criterion specified for automatic local subdivision of the independent variable, it was found that there was no change in the fifth decimal place of $f''(0)$, $\phi'(0)$, I_w and $f(\infty)$ for $\eta_{\text{edge}} = 20$, $\Delta\eta = 0{\cdot}05$ and a value of 10^{-10} for the predictor–corrector accuracy criterion. Under these conditions, at η_{edge},

$$f' \approx 10^{-12} \quad \text{and} \quad \phi \approx 10^{-20} \quad \text{and} \quad \int_0^{\eta_{\text{edge}}} W/I_w = 1 \pm 0{\cdot}000001.$$

The resulting calculated transport parameters are listed in table 2 for the values of σ, q and R given above. The Prandtl number range considered, $8{\cdot}6 \leqslant \sigma \leqslant 13{\cdot}6$, and the range of pressure and/or salinity effects on q cover a very wide range of actual

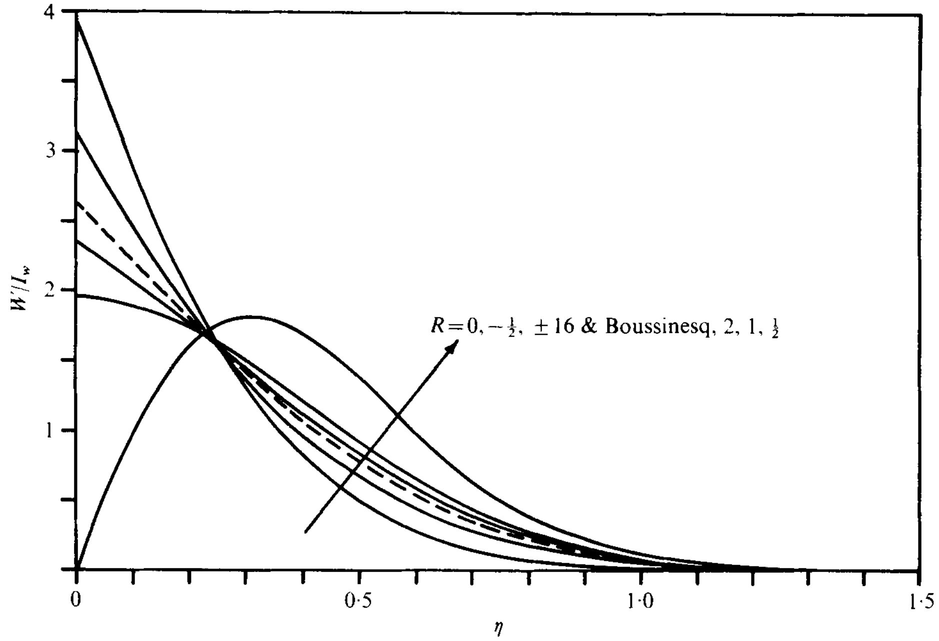

FIGURE 8. Calculated distribution of local buoyancy force for selected values of R, $\sigma = 11{\cdot}6$ and $q(s,p) = q(0,1) = 1{\cdot}894816$.

conditions. The upper section (a) of table 2 shows the Prandtl number effect on transport and the lower section (b) shows the effect of the pressure and/or salinity level.

For $\sigma = 11{\cdot}6$ and $q(s,p) = q(0,1)$, the vertical component of velocity adjacent to the surface is shown in figure 5 for various values of R. Recall that the flow is upward for $R \leqslant 0$ and downward for $R \geqslant \frac{1}{2}$. The dashed curve represents the conventional Boussinesq results. The magnitude of the maximum of $f'(\eta)$ is seen to increase by about 60% from $R = 0$ to $R = \frac{1}{2}$. Large calculated differences from conventional results are apparent.

A much smaller effect on the calculated temperature distribution, in our coordinates, is seen in figure 6. Higher temperature gradients near the surface correspond to vertical (downward) velocity components of larger magnitude. The corresponding horizontal (inward) velocity component is shown in figure 7. A 40% decrease in the entrainment velocity is seen between $R = \frac{1}{2}$ and $R = 0$. These changes are related to those in the vertical velocity component seen in figure 5.

The distribution of the normalized local buoyancy force $W(\eta)/I_w$ is shown in figure 8. For $R = 0$, the upper bound for a uniformly upward buoyancy force, the buoyancy force is larger at the surface than for the other conditions shown. This corresponds to a higher calculated average fluid temperature distribution and associated lower velocity levels. For $R = \frac{1}{2}$, the lower bound for a uniformly downward buoyancy force is zero at the surface and has an extremum at $\eta \approx 0{\cdot}3$. Recall that I_w is always negative for $R \geqslant \frac{1}{2}$ (downflow) and positive for $R \leqslant 0$ (upflow), and that

$$\int_0^\infty W(\eta)\, d\eta \equiv I_w.$$

	(a)						(b)		
R	$\sigma = 8{\cdot}6$	$\sigma = 9{\cdot}6$	$\sigma = 10{\cdot}6$	$\sigma = 11{\cdot}6$	$\sigma = 12{\cdot}6$	$\sigma = 13{\cdot}6$	$q(0, 100)$	$q(0, 500)$	$q(0, 1000)$
−16·00	2·45117	2·53026	2·60322	2·67105	2·73451	2·79421	2·59421	2·32197	2·05462
−14·00	2·38025	2·45705	2·52790	2·59376	2·65538	2·71335	2·52206	2·26723	2·01569
−12·00	2·30113	2·37538	2·44387	2·50754	2·56711	2·62314	2·44145	2·20578	1·97178
−10·00	2·21126	2·28260	2·34841	2·40960	2·46683	2·52067	2·34977	2·13550	1·92125
−8·00	2·10655	2·17452	2·23721	2·29548	2·35000	2·40129	2·24276	2·05293	1·86146
−4·00	1·81651	1·87508	1·92911	1·97935	2·02634	2·07052	1·94515	1·82000	1·69011
−3·00	1·71096	1·76611	1·81698	1·86427	1·90853	1·95014	1·83638	1·73350	1·62538
−2·00	1·57626	1·62704	1·67387	1·71742	1·75815	1·79647	1·69715	1·62159	1·54064
−1·00	1·38283	1·42730	1·46833	1·50647	1·54215	1·57571	1·49628	1·45739	1·41402
−0·50	1·23420	1·27380	1·31033	1·34429	1·37606	1·40594	1·34098	1·32770	1·31164
0·00	0·96210	0·99263	1·02079	1·04696	1·07144	1·09447	1·05222	1·07289	1·09707
0·50	0·94073	0·97181	1·00047	1·02713	1·05207	1·07553	1·03156	1·04794	1·06494
1·00	1·22606	1·26589	1·30264	1·33680	1·36877	1·39883	1·33368	1·32118	1·30604
2·00	1·48633	1·53443	1·57881	1·62006	1·65867	1·69497	1·60458	1·54633	1·48293
3·00	1·64551	1·69872	1·74780	1·79342	1·83611	1·87626	1·76927	1·67972	1·58479
4·00	1·76423	1·82124	1·87383	1·92273	1·96848	2·01150	1·89167	1·77756	1·65843
8·00	2·07606	2·14310	2·20496	2·26246	2·31626	2·36685	2·21174	2·02891	1·84398
10·00	2·18562	2·25619	2·32130	2·38182	2·43845	2·49172	2·32375	2·11547	1·90679
12·00	2·27886	2·35245	2·42033	2·48343	2·54248	2·59801	2·41890	2·18853	1·95941
14·00	2·36049	2·43671	2·50702	2·57238	2·63354	2·69106	2·50207	2·25202	2·00486
16·00	2·43337	2·51193	2·58441	2·65178	2·71483	2·77410	2·57623	2·30834	2·04495

TABLE 3. Calculated values of $-\phi'(0)|I_w|^{\frac{1}{4}} = \frac{3}{4} \times 2^{\frac{1}{4}}\overline{Nu_L}/Gr_L'^{\frac{1}{4}}$ for (a) $q(s,p) = q(0,1) = 1{\cdot}894816$ and $\sigma = 8{\cdot}6$, $9{\cdot}6$, $10{\cdot}6$, $11{\cdot}6$, $12{\cdot}6$ and $13{\cdot}6$ and (b) $\sigma = 11{\cdot}6$ and $q(s,p) = q(0,100) = 1{\cdot}859663$, $q(0,500) = 1{\cdot}727147$ and $q(0,1000) = 1{\cdot}582950$.

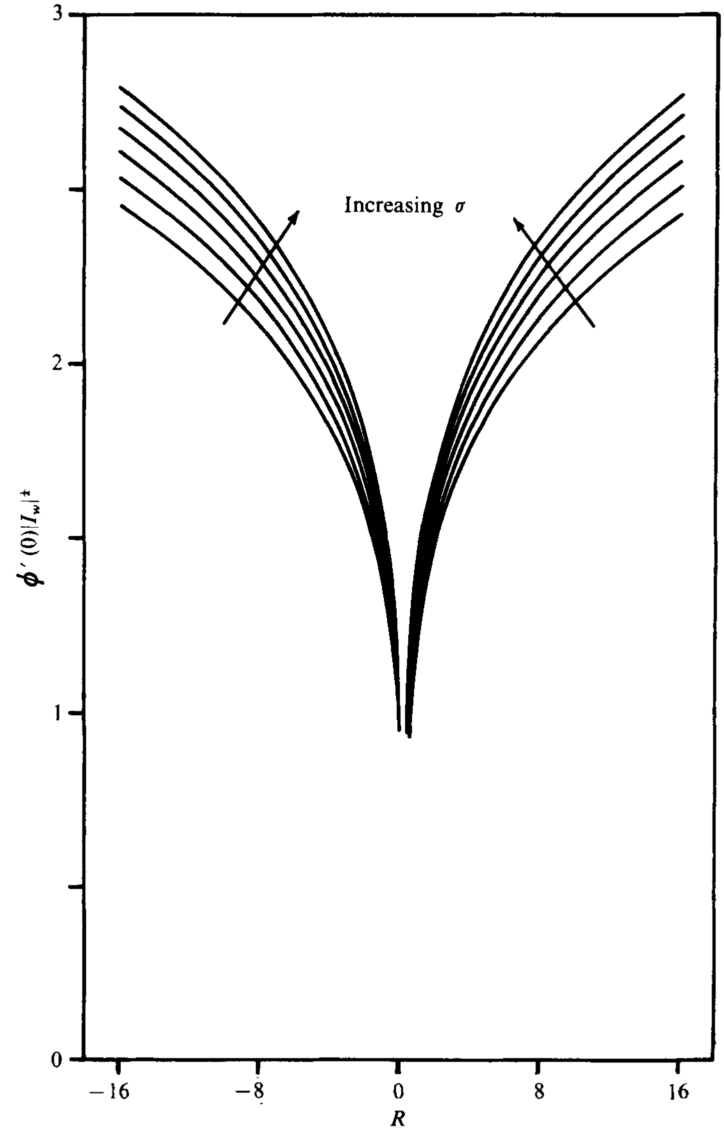

FIGURE 9. Heat-transfer dependence on R. The six curves were calculated for σ = 8·6, 9·6, 10·6, 11·6, 12·6 and 13·6, increasing in the direction shown. Results are for $q(s, p) = q(0, 1) = 1{\cdot}894816$.

From (43), the average Nusselt number $Nu_L = \bar{h}L/k$ for a surface of vertical extent L is given by

$$\frac{Nu_L}{Gr_L'^{\frac{1}{4}}} = \frac{4}{3\times 2^{\frac{1}{2}}}[-\phi'(0)][|I_w|]^{\frac{1}{4}}, \tag{44}$$

where Gr_L' is defined by (29). Values of $[-\phi'(0)]\,[|I_w|]^{\frac{1}{4}}$ have been computed from the results shown in table 2 for the same values of σ, q and R and are shown in table 3. The effect of the Prandtl number on this heat-transfer parameter is also shown in figure 9. As the Prandtl number decreases from 13·6 to 8·6, there is a decrease in heat transfer at all R. The total decrease is uniformly about 14 %. For each Prandtl number,

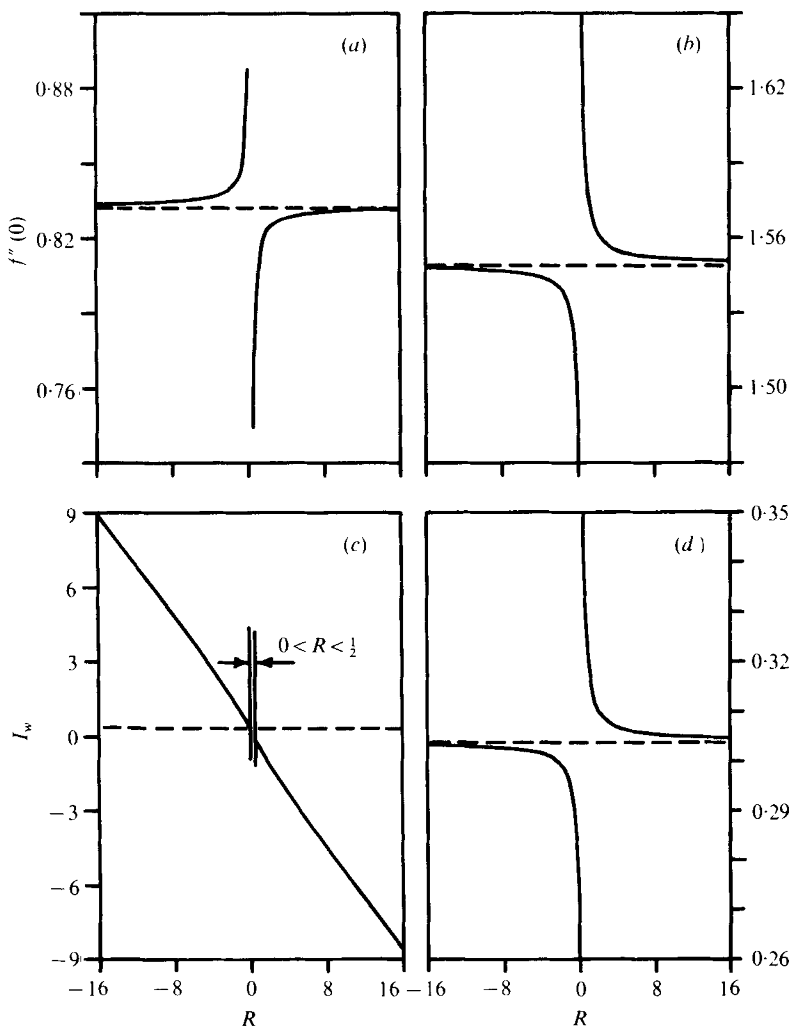

FIGURE 10. (a) Drag $f''(0)$, (b) heat transfer $-\phi'(0)$, (c) net buoyancy I_w and (d) mass flow rate $f(\infty)$ over the range of R for $\sigma = 11{\cdot}6$ and $q(s,p) = q(0,1) = 1{\cdot}894816$. Horizontal dashed lines are Boussinesq asymptotes.

a striking decrease in heat transfer is seen as R approaches the region of buoyancy-force reversal. These large effects are not limited to low temperature levels. For example, $R = 0{\cdot}6$ in pure water at atmospheric pressure for $t_0 = 20$ °C and $t_\infty = 10$ °C. This may also be looked upon as a consequence of the strong variation of β with temperature, by about a factor of 6·5 from 6 to 20 °C.

As will be seen later, the variation of I_w with R is smooth and nearly linear, with $I_w < 0$ for $-16 \leqslant R \leqslant 0$ and $I_w > 0$ for $\frac{1}{2} \geqslant R \geqslant 16$. These trends confirm the surmise that $I_w = 0$ occurs in the region $0 < R < \frac{1}{2}$ and suggest that we might initially infer its behaviour in this range from the calculated smooth behaviour outside.

From such plots of I_w as a function of R, which amplify the region near $I_w = 0$, convective reversal was inferred to occur at $R = 0{\cdot}310 \pm 0{\cdot}001$. This value applies over the whole range of Prandtl numbers considered, $8{\cdot}6 \leqslant \sigma \leqslant 13{\cdot}6$. For a vertical

σ	$f''(0)$	$-\phi'(0)$	I_w	$f(\infty)$
8·6	0·81002	1·38014	0·43301	0·32028
9·6	0·81838	1·44036	0·41447	0·31412
10·6	0·82565	1·49646	0·39858	0·30871
11·6	0·83204	1·54908	0·38475	0·30390
12·6	0·83773	1·59870	0·37256	0·29958
13·6	0·84283	1·64572	0·36171	0·29566

TABLE 4. Heat-transfer and flow parameters $f''(0)$, $-\phi'(0)$, I_w and $f(\infty)$ as calculated using the Boussinesq approximation for $\sigma = 8{\cdot}6$, $9{\cdot}6$, $10{\cdot}6$, $11{\cdot}6$, $12{\cdot}6$ and $13{\cdot}6$.

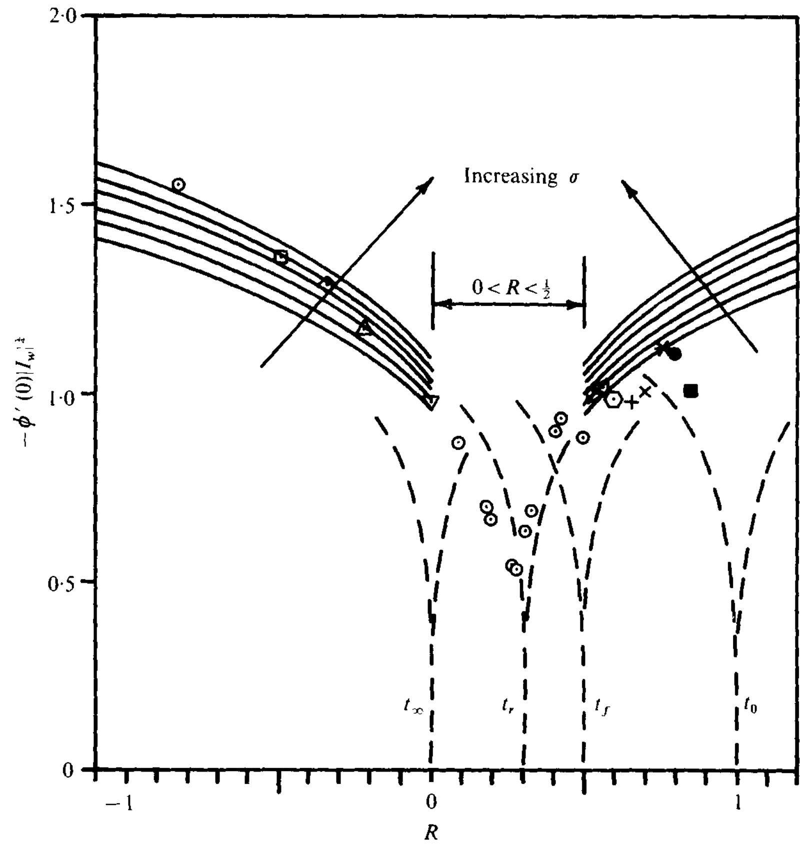

FIGURE 11. Calculated heat-transfer variation with R near the region of net buoyancy-force reversal compared with the measurements by Bendell & Gebhart (1976). Calculated results in figure 9 are here compared with those obtained using the Boussinesq approximation with β evaluated at various temperatures. For symbols see table 5.

surface at 0 °C in pure water we predict convective inversion to occur at an ambient temperature $t_\infty = 5{\cdot}8$ °C when t_m is taken as 4·029 °C. Measurements by Bendell & Gebhart (1976) report upflow for $t_\infty = 5{\cdot}5$ °C and downflow for $t_\infty = 5{\cdot}6$ °C.

Our calculations also showed that, as the condition of net buoyancy-force reversal was approached, the non-dimensional surface shear, heat flux and mass flow rate

t_∞	R	Pr at t_f	$Gr'_L = g\alpha L^3 \lvert t_0 - t_\infty \rvert^q / \nu^2$ at t_f	$\overline{Nu}_L$ (exp.)	$-\phi'(0) \lvert I_w \rvert^{\frac{1}{4}}$ (exp.)	Symbols in figure 11	$-\phi'(0) \lvert I_w \rvert^{\frac{1}{4}}$ (theor.)	% deviation
25·2	0·841	8·6	$7{\cdot}82 \times 10^8$	172·5	1·006	■	1·16	−15·3
19·9	0·798	9·3	$4{\cdot}33 \times 10^8$	163·4	1·104	●	1·17	−6·0
16·9	0·762	9·8	$2{\cdot}87 \times 10^8$	149·1	1·115	✳	1·16	−4·0
13·3	0·697	10·3	$1{\cdot}67 \times 10^8$	116·9	1·001	×	1·14	−13·9
11·7	0·656	10·6	$1{\cdot}23 \times 10^8$	105·2	0·972	+	1·12	−15·2
10·1	0·601	10·9	$9{\cdot}02 \times 10^7$	98·4	0·982	⬡	1·09	−10·9
9·1	0·557	11·1	$7{\cdot}20 \times 10^7$	96·4	1·018	◁	1·07	−5·1
8·5	0·526	11·2	$6{\cdot}06 \times 10^7$	90·6	0·999	▷	1·04	−4·1
8·0	0·496	11·3	$5{\cdot}34 \times 10^7$	77·5	0·882	○	—	—
7·0	0·424	11·5	$4{\cdot}10 \times 10^7$	76·8	0·933	○	—	—
6·8	0·407	11·7	$3{\cdot}79 \times 10^7$	72·4	0·898	○	—	—
6·0	0·328	11·7	$2{\cdot}97 \times 10^7$	52·1	0·686	○	—	—
5·8	0·305	11·7	$2{\cdot}69 \times 10^7$	46·7	0·631	○	—	—
5·6	0·280	11·8	$2{\cdot}58 \times 10^7$	38·9	0·531	○	—	—
5·5	0·267	11·8	$2{\cdot}48 \times 10^7$	39·4	0·543	○	—	—
5·0	0·194	11·9	$2{\cdot}00 \times 10^7$	45·9	0·667	○	—	—
4·9	0·178	11·9	$1{\cdot}92 \times 10^7$	47·6	0·699	○	—	—
4·4	0·084	12·0	$1{\cdot}54 \times 10^7$	55·8	0·866	○	—	—
4·0	−0·007	12·1	$1{\cdot}30 \times 10^7$	60·0	0·972	▽	1·05	−8·0
3·3	−0·221	12·3	$8{\cdot}80 \times 10^6$	65·3	1·166	△	1·22	−4·6
3·0	−0·343	12·3	$7{\cdot}13 \times 10^6$	68·2	1·284	◇	1·29	−0·4
2·7	−0·492	12·4	$5{\cdot}91 \times 10^6$	68·8	1·357	□	1·37	−1·0
2·2	−0·832	12·5	$3{\cdot}87 \times 10^6$	70·5	1·546	○	1·49	−3·6
								−6·5 % avg.
								8·6 % r.m.s.

TABLE 5. Comparison of the data of Bendell & Gebhart (1976) and the present calculated results.

parameters $f''(0)$, $-\phi(0)$ and $f(\infty)$, respectively, diverged to large positive values on one side of $0 < R < \frac{1}{2}$ and large negative values on the other side. This characteristic required increased care in the numerical calculations as the region $0 < R < \frac{1}{2}$ was approached. The variation of $f''(0)$, $-\phi'(0)$, I_w and $f(\infty)$ with R is shown in figure 10 for $\sigma = 11{\cdot}6$ and $q(s,p) = q(0,1)$. The asymptotes associated with conventional analysis, for each of $f''(0)$, $\phi'(0)$, I_w and $f(\infty)$, are shown as dashed lines. Except for I_w, the curves are strikingly similar, in that they diverge rapidly near $R = 0$ and $R = \frac{1}{2}$. At large $|R|$ they closely approach the asymptotes for $R = 0$ and $q = 1$, which are given in table 4. Note that I_w decreases almost linearly as R increases.

Figure 11 shows the heat-transfer variation expanded for the region of R in which convective inversion occurs. The solid curves again represent present results, for $8{\cdot}6 \leqslant \sigma \leqslant 13{\cdot}6$, all for $q = q(0,1)$. Also shown are the data of Bendell & Gebhart (1976), corrected for an error in data reduction, which cover a Prandtl number range of from 8·6 to 12·5. The particular Grashof number Gr_L used in their paper has been converted to Gr'_L, as shown in table 5. The heat-transfer data in the region of our calculations agree to within an average difference of $-6{\cdot}5\,\%$ with present results. Inside $0 < R < \frac{1}{2}$, the data seen to lie on reasonable extrapolations of our computed results. The Prandtl number trend in the data also agrees with the calculated Prandtl number effect. The maximum deviation between measured and calculated results is about 15 %. The r.m.s. is only 8·6 %.

The theory compared with data in figure 11 do not include an allowance for interface motion, or equivalently, interface blowing, in the boundary condition $f(0)$ in (39). This is to be expected. One may show from continuity considerations and from (40) that the proper value of $f(0)$ is less than $c_p(t_\infty - t_{il})/\sigma h_{il}$, where h_{il} is the latent heat of fusion. For water, this parameter has a value of less than 10^{-3}. Since consequent changes in $\phi'(0)$ would be of comparable order, the above comparison of present results with these data is appropriate.

It is of interest to compare our results with those which result from using the conventional approximation for the density difference. These are equivalent to the present formulation for $|R| \to \infty$ and also for $R = 0$ and $q = 1$. Recall that a single value of β cannot correctly reflect the consequences of a density extremum. The conventional formulation for heat transfer is

$$Nu_L = \frac{4}{3 \times 2^{\frac{1}{2}}}\left[\frac{g\beta L^3(t_0 - t_\infty)}{\nu^2}\right]^{\frac{1}{4}}[-\phi'(0)]_B. \tag{45}$$

We consider the possibility of modifying this to represent more correctly the behaviour near the density extremum, using some reference temperature to evaluate β. From (20), β is calculated as

$$\beta_r = \alpha q(\rho_m/\rho_r)\,|t_r - t_m|^{q-1}, \tag{46}$$

where the subscript r refers to conditions at a suitably chosen reference temperature t_r. Since the physical heat transfer is independent of the formulation, we equate the two forms (44) and (45) for Nu_L and obtain

$$[-\phi'(0)]\,[|I_w|]^{\frac{1}{4}} = \left[q\left(\frac{\rho_m}{\rho_r}\right)\left|\frac{t_r - t_m}{t_0 - t_\infty}\right|^{q-1}\right]^{\frac{1}{4}}[-\phi'(0)]_B, \tag{47}$$

where the subscript B indicates the conventional value calculated using the Grashof number contained in (45). It remains to determine a reasonable reference temperature

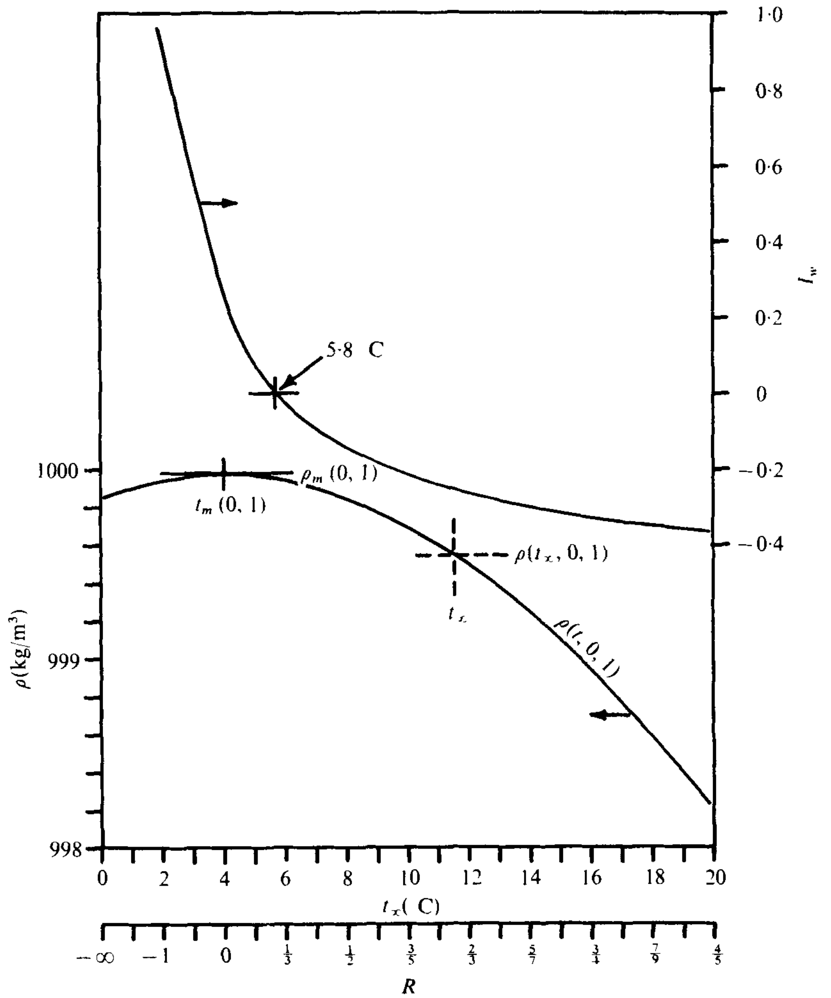

FIGURE 12. Variation of density and calculated net buoyancy force with temperature and R for a surface at 0 °C in pure water at t_∞ and $q(s,p) = q(0,1) = 1{\cdot}894816$, for $\sigma = 11{\cdot}6$.

for β. Choosing t_r successively at three different levels t_∞, t_0 and $t_f \equiv \frac{1}{2}(t_0+t_\infty)$, (47) becomes

$$[-\phi'(0)][|I_w|]^{\frac{1}{4}} = [q(\rho_m/\rho_\infty)\,|R|^{q-1}]^{\frac{1}{4}}[-\phi'(0)]_B, \tag{48a}$$

$$[-\phi'(0)][|I_w|]^{\frac{1}{4}} = [q(\rho_m/\rho_0)\,|1-R|^{q-1}]^{\frac{1}{4}}[-\phi'(0)]_B, \tag{48b}$$

$$[-\phi'(0)][|I_w|]^{\frac{1}{4}} = [q(\rho_m/\rho_f)\,|\tfrac{1}{2}-R|^{q-1}]^{\frac{1}{4}}[-\phi'(0)]_B. \tag{48c}$$

These three results are shown as the dashed lines on figure 11, for $q = q(0,1)$. Note that each of these distributions is similar to the trend of the present formulation (solid lines). However they are displaced.

The two methods may be brought into closer agreement in the region of net buoyancy-force reversal if we choose the reference temperature as

$$t_r = t_0 - 0{\cdot}69(t_0 - t_\infty). \tag{49}$$

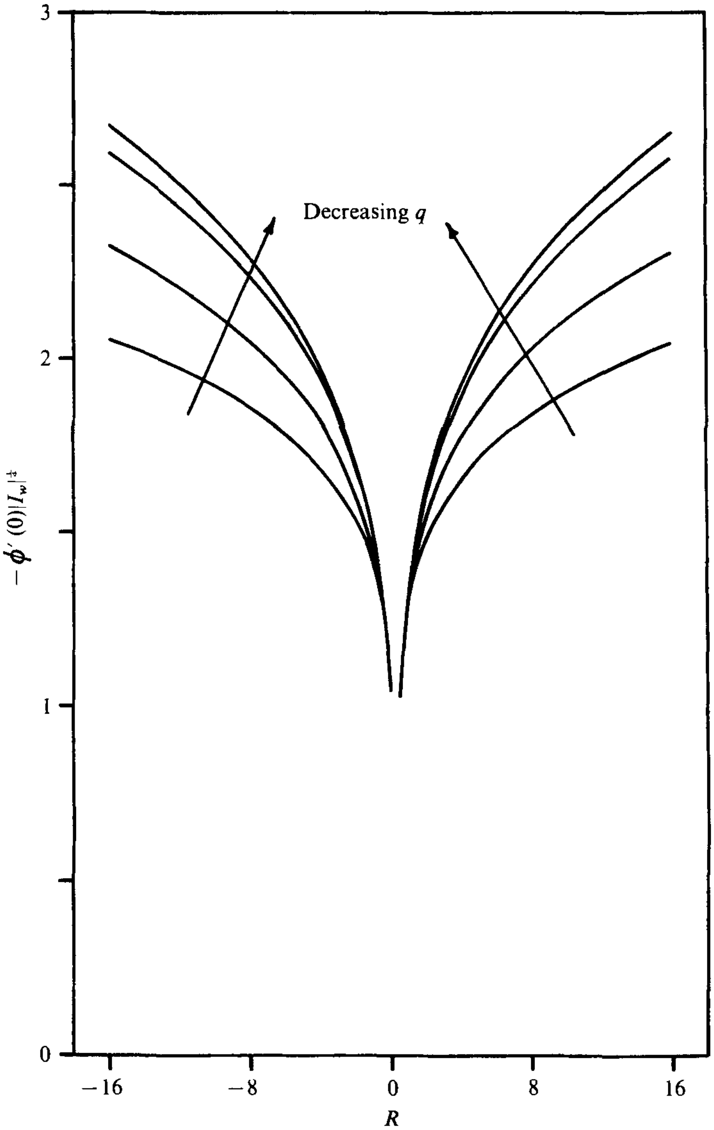

FIGURE 13. Calculated effect of pressure and/or salinity level on heat transfer for a range of R, $\sigma = 11{\cdot}6$ and $q(0,1)$, $q(0,100)$, $q(0,500)$, $q(0,1000)$. These numerical values of $q(0,p)$ are given in table 2.

Then (47) becomes

$$[-\phi'(0)]\,[|I_w|]^{\frac{1}{4}} = [q(\rho_m/\rho_r)\,|R-0{\cdot}31|^{q-1}]^{\frac{1}{4}}\,[-\phi'(0)]_B. \qquad (50)$$

This result is also plotted on figure 11, for $\sigma = 11{\cdot}6$ and $q = q(0,1)$. Therefore the conventional results will agree with present ones when an accurate expression for β, viz. (46), is used with a proper choice of t_r. If t_r is chosen for best agreement with the data of Bendell & Gebhart (1976), then the value of 0·69 in (49) should be 0·72.

We shall now consider the physical interpretation of buoyancy-force reversal and convective inversion. Consider a vertical surface at $t_0 = 0$ °C. Figure 12 shows the density variation with temperature out through the thermal region. Also shown is the variation of the net buoyancy force I_w, determined by interpolation, as it decreases with increasing choices of t_∞ above 0 °C. The corresponding values of R are also shown on the abscissa. We see that $I_w = 0$ corresponds to about $t_\infty = 5{\cdot}8$ °C at $R = 0{\cdot}31$ for $\sigma = 11{\cdot}6$ and $q = q(0, 1)$. For $t_\infty > 5{\cdot}8$ °C the flow is predicted to be downward while for $t_\infty < 5{\cdot}8$ °C the flow is predicted to be upward, if it is not bi-directional.

Finally, the calculated effect of q, i.e. of the pressure and/or salinity level, on heat transfer is shown in figure 13. Results are plotted for $\sigma = 11{\cdot}6$ over a wide range of R. The values of q cover its variation over the range $1 < p < 1000$ bar abs. and

$$0 < s < 40\,\text{p.p.t.}$$

Decreasing $q(s,p)$ is seen to decrease heat transfer by about 23% at large $|R|$. As the condition of net buoyancy-force reversal is approached, there remains a sharp decrease in heat transfer for all q.

Throughout the foregoing calculations we have used the precise numerical values of q which relate to the easily identifiable conditions $q(0, 1)$, $q(0, 100)$, $q(0,500)$ and $q(0, 1000)$. The summarized results in table 2 are then very accurate for these specific conditions, for any subsequent uses which may arise. Here we use these results to estimate the effects of rounding q down from the values obtained from the correlation (20) in table 6. The effect of q is largest at large $|R|$. Certainly I_w is the most sensitive of the transport parameters. The results in table 2, for $R = \pm 16$, indicate that I_w decreases by about 30 parts per one part decrease in $q(s,p)$. As a result, a change in I_w of 0·1% accompanies a change in the value of q of about 0·0003. Thus, for example, $q(0, 500) = 1{\cdot}727147$ may be rounded to 1·7271 without affecting accuracy to 0·1% in I_w.

6. Combined thermal and saline diffusion: conditions for similarity

The parameter R includes the effect of density inversion. It also eliminates the need for any approximation for the buoyancy force, which becomes simply as given in (26c). This is exact, inasmuch as is the equation of state for density. The other role of R is to locate the density maximum in the ϕ distribution, as dictated by the relation of t_0 and t_∞ to t_m.

Admitting simultaneously the t, s and p effects on density, equation (20), makes the formulation of buoyancy more complicated. However, we have seen in a previous section that the pressure effect is often small. Then only the pressure level that pertains in a given flow or configuration enters the formulation. We further elect to use here the simpler state equation, for $n = 2$, which contains no s^2 terms. Also, since there is no s term in q, $q(s,p)$ becomes $q(p)$.

The values p and s_∞ determine the constant values of $\rho_m(s_\infty, p)$, $\alpha(s_\infty, p)$ and $t_m(s_\infty, p)$ which apply for any particular application of the present results. As a result, the only variables in the buoyancy force are t and s, as given in (20). This is particularly convenient in analysis since there is only one t term and ρ_m, α and t_m are each only linearly dependent on s. As a result there will be few circumstance-dependent parameters in the buoyancy force, apart from R. The s^2 terms in (21)–(24) may be retained for higher accuracy, with additional complexity.

However, the detailed mechanics of flows which have salinity gradients are very much more complicated. The joint effects of the local values of t and s determine the distribution of ρ across the convection region, through (20). The t and s distributions, on the other hand, are governed by the full set (15)–(17), along with the relevant boundary conditions.

As an example, consider a vertical surface freezing water from a saline ambient medium at, say, $t_\infty = 2t_m$. The local temperature decreases into the thermal layer. This will cause a local density maximum and then decreasing density before the much thinner saline diffusion region is reached. Recall that the Lewis number α_t/D, where α_t is the thermal diffusivity, is about 100. Since dissolved salt is largely excluded in freezing, the salinity level will be higher nearer to the interface, in the thin region of salinity diffusion. For appreciable values of the difference $s_0 - s_\infty$, the density again begins to increase. The result is a local minimum. Thus multiple extrema may occur in quite ordinary circumstances.

The buoyancy density difference is calculated from $\rho(t, s, p)$ in (20). There are no terms in the salinity squared:

$$\frac{\rho_\infty - \rho}{\rho_m(s_\infty, p)\,\alpha(s_\infty, p)\,|t_0 - t_\infty|^q} = [1 + AS][1 + BS]|\phi - R - QS|^q - |R|^q - PS \tag{51}$$
$$= W(\eta, \phi, S, A, B, R, P, Q, q),$$

where

$$R = \frac{t_m(s_\infty, p) - t_\infty}{t_0 - t_\infty} = \frac{T_m - t_\infty}{t_0 - t_\infty}, \tag{52a}$$

$$A' \equiv A/\Delta s_0 \equiv g_1(p)\,\rho_m(0,1)/\rho_m(s_\infty, p), \tag{52b}$$

$$B' \equiv B/\Delta s_0 \equiv g_2(p)\,\alpha(0,1)/\alpha(s_\infty, p), \tag{52c}$$

$$Q' \equiv Q\Delta t_0/\Delta s_0 \equiv g_3(p)\,t_m(0,1), \tag{52d}$$

$$P' \equiv P|\Delta t_0|^q/\Delta s_0 \equiv g_1(p)\,\rho_m(0,1)/\alpha(s_\infty, p)\,\rho_m(s_\infty, p) = A'/\alpha(s_\infty, p), \tag{52e}$$

where T_m denotes the extremum temperature under the conditions in the local ambient medium. The additional parameters which have arisen in W, owing to saline diffusion, are A, B, Q and $P = A/\alpha d^q$. The magnitudes of A and B are usually small compared with 1. They are primarily the effects of the local ambient-medium salinity level on the level of ρ_m and α. On the other hand, PS is the principal component of the contribution of the salinity gradient to the buoyancy force. We see from (52*b*) that this is a very large term for $s_0 - s_\infty$ large. This gives a large effect of $\rho_\infty - \rho$ compared with the temperature effect. However, the salinity diffusion layer is very thin. The other salinity contribution, Q, is the effect of the salinity gradient on t_m. Although the term QS may be larger than ϕ, for $s_0 - s_\infty$ large, the range of its effect, in η, is also small.

There are several separate physical effects in this formulation. We have already discussed, for thermally driven flows, the effect on transport of the ambient-medium salinity and pressure level. The new effects are seen in the eventual equations below and are those of salinity level and diffusion in F in (53*a*), in conjunction with (53*c*). The effects of these levels are contained in A and B. Their signs are determined by that of $s_0 - s_\infty$. The sign of the strong buoyancy effect $-PS$ also follows that of $s_0 - s_\infty$. This has to do with the temperature and salinity buoyancy effects tending to oppose or aid each other. This tendency, however, is mediated by the relative magnitude of

ϕ compared with $-(R+QS)$ and by their difference compared with R. Here QS is the shift in the local density extremum temperature across the thin region of saline diffusion.

Similarity solutions may again be found, with simultaneous saline diffusion, for a broad range of important practical applications in low temperature water. The equations are again (15) and (16) with (51) as the buoyancy force and (17) added for salinity diffusion. The conditions on b and c are (28) as before and Gr_x may be defined as in (29). However, we may still normalize W by I_w [see (30)] as was done in (32) and use (51) to obtain $F(\eta)$. Then Gr_x is given by (31) instead.

Here we consider a simple case with neither temperature nor salinity stratification, i.e. t_∞ and s_∞ uniform. The surface conditions t_0 and s_0 will also be taken uniform. Neglecting the pressure and viscous dissipation energy effects, the equations in f, ϕ and S become

$$f''' + 3ff'' - 2f'^2 + F = 0, \tag{53a}$$

$$\phi'' + 3\sigma f\phi', \quad S'' + 3ScfS' = 0, \tag{53b, c}$$

where $S = (s-s_\infty)/(s_0-s_\infty)$ and again F is W in (51) divided by I_w. The set of boundary conditions for an impermeable surface and no slip is

$$f'(0) = f(0) = 1-\phi(0) = 1-S(0) = f'(\infty) = \phi(\infty) = S(\infty) = 0. \tag{53d}$$

Again this combined buoyancy-mode formulation has similar solutions, as did the simpler thermal buoyancy formulation above, for conditions where W is independent of x. This question is assessed in (51) and (52). We note that A, B, Q, P, q and R are all independent of x if t_0, t_∞, s_0 and s_∞ are uniform and any effect of pressure variation on the density level is neglected. Thus the only difference with saline diffusion is that W is now defined as in (51) and (52).

This permits the similarity analysis of many important transport mechanisms. There are, in addition, other solutions for special circumstances and approximations concerning the effects of salinity and melting and freezing.

7. Conclusions

This analysis of thermal, momentum and saline transport is more general than those in the past. The effect of high levels of salinity and pressure are simply included in a single formulation. Very few circumstance-dependent parameters arise in this treatment, which permits complete flexibility of the temperature conditions up to 20 °C. This results from a very accurate new equation of state whose single temperature term confers simplicity. There is no additional approximation in the calculation of the buoyancy force to the level of accuracy of the most recent wide-range fundamental density data. This accuracy of representation applies across the regions containing extrema as well as for the temperature, salinity and pressure conditions in the vast majority of terrestrial surface water.

We have treated vertical flows generated adjacent to surfaces. Extensive calculations were made for thermally buoyant flows. The results indicate that very large errors in transport prediction arise from the conventional approximation of linearizing the temperature dependence of density in the buoyancy force.

The calculations also show that the substantial variation of the Prandtl number

j	0	1	2	3
f_{1j}	—	$4{\cdot}960998E-05$	$-2{\cdot}601973E-09$	$7{\cdot}842619E-13$
f_{2j}	—	$1{\cdot}377584E-04$	$1{\cdot}497648E-06$	$2{\cdot}903240E-10$
f_{3j}	—	$-5{\cdot}430000E-03$	$7{\cdot}720181E-07$	$-7{\cdot}038846E-10$
f_{4j}	—	$-1{\cdot}118758E-04$	$-1{\cdot}238393E-07$	$5{\cdot}857253E-11$
g_{1j}	$7{\cdot}992252E-04$	$-5{\cdot}194896E-08$	$1{\cdot}031185E-10$	$-2{\cdot}979653E-14$
g_{2j}	$1{\cdot}623355E-02$	$1{\cdot}129961E-05$	$-8{\cdot}053248E-08$	$6{\cdot}966452E-12$
g_{3j}	$-5{\cdot}265509E-02$	$7{\cdot}496781E-05$	$-2{\cdot}792053E-07$	$1{\cdot}411138E-10$
g_{4j}	$-3{\cdot}136530E-03$	$2{\cdot}983937E-06$	$4{\cdot}453557E-09$	$-2{\cdot}937601E-12$
h_{1j}	$1{\cdot}918334E-07$	$1{\cdot}347190E-09$	$-2{\cdot}203133E-12$	$1{\cdot}112440E-15$
h_{2j}	$-4{\cdot}565866E-04$	$-4{\cdot}352912E-07$	$1{\cdot}978675E-09$	$-9{\cdot}079379E-13$
h_{3j}	$0{\cdot}000000$	$-3{\cdot}683650E-06$	$7{\cdot}694077E-09$	$-4{\cdot}561113E-12$
h_{4j}	$7{\cdot}599378E-05$	$-8{\cdot}718915E-08$	$-4{\cdot}166570E-11$	$5{\cdot}870105E-14$

TABLE 6. The parameters in (20) for $n = 3$. $\alpha(0, 1) = 9{\cdot}297173E-06$ $(^{\circ}\mathrm{C})^{q}$, $t_m(0, 1) = 4{\cdot}029325E+00$ °C, $q(0, 1) = 1{\cdot}894816E+00$ °C.

over the relevant temperature range, principally through viscosity variation. causes appreciable additional effects on transport. The salinity and pressure levels in the flow field also have considerable effects. These are included simply in the three salinity- and pressure-dependent parameters which arise. Two of these parameters occur in a new form of the local Grashof number. This form is a very much more accurate measure of local flow vigour and direction than the conventianal one.

Density extrema have large effects on transport. Under some conditions buoyancy-force reversals arise. This leads eventually to zero net buoyancy and then to convective inversion. One of the most significant results is the ability of this formulation to localize the condition for convective inversion. All our predictions are in close accord with experiments.

The last section shows that similarity solutions also result for flows arising from the combined buoyancy effects of simultaneous thermal and saline diffusion over a wide range of salinities and pressures. Several additional salinity- and pressure-dependent parameters arise. Their relative importance is discussed in terms of their magnitudes and domains of importance in determining transport. The occurrence of multiple density extrema in some flow configurations is apparent.

The authors wish to acknowledge support for this study by the National Science Foundation under research grants GK18529, ENG75-05466 and ENG75-22623 (first author) and ENG76-16936 (second author). The second author further acknowledges support from the Research Foundation of the State University of New York and SUNY/Buffalo Institutional Funds. Both authors would also like to thank Bonnie Boskat for her expert efforts in the preparation of the manuscript.

Appendix. The density correlation

We append here, for convenient access and in sufficient detail for use, both the most accurate and the simplest of the correlations found by Gebhart & Mollendorf (1977). The (0, 1) values and the coefficients in the following pressure polynomials

j	0	1	2
f_{1j}	—	$4{\cdot}955317E-05$	$-1{\cdot}950180E-09$
f_{2j}	—	$5{\cdot}181147E-04$	$1{\cdot}190039E-06$
f_{3j}	—	$-5{\cdot}430000E-03$	$2{\cdot}455177E-07$
f_{4j}	—	$-1{\cdot}898839E-04$	$2{\cdot}515528E-08$
g_{1j}	$8{\cdot}046157E-04$	$-1{\cdot}051410E-09$	$3{\cdot}304577E-11$
g_{2j}	$-2{\cdot}839092E-03$	$-7{\cdot}125734E-06$	$-2{\cdot}430584E-09$
g_{3j}	$-5{\cdot}265509E-02$	$-6{\cdot}824758E-05$	$2{\cdot}106695E-09$

TABLE 7. A simpler correlation, for $n = 2$.

have been rounded to an extent which does not affect $\rho(t, s, p)$ by more than 0·1 p.p.m. over the whole range of conditions:

$$f_i(p) = \sum_{j=1}^{n} f_{ij}(p-1)^j, \quad g_i(p) = \sum_{j=0}^{n} g_{ij}(p-1)^j, \qquad \text{(A 1), (A 2)}$$

$$h_i(p) = \sum_{j=0}^{n} h_{ij}(p-1)^j. \qquad \text{(A 2)}$$

Values of the coefficients are given in table 6 for the most accurate correlation at $n = 3$, retaining all pressure functions, and in table 7 for $n = 2$ with no s^2 terms and no s term in the exponent q.

REFERENCES

BENDELL, M. S. & GEBHART, B. 1976 Heat transfer and ice-melting in ambient water near its density extremum. *Int. J. Heat Mass Transfer* **19**, 1081–1087.

CALDWELL, D. R. 1977 The maximum-density points of saline water. Submitted to *Deep-Sea Res.*

CHEN, C. T. & MILLERO, F. J. 1976 The specific volume of sea water at high pressures. *Deep-Sea Res.* **23**, 595–612.

CODEGONE, C. 1939 Su un punto d'inversione dei moti convettivi. *Acad. Sci. Torino* **75**, 167.

DOHERTY, B. T. & KESTER, D. R. 1974 Freezing point of seawater. *J. Mar. Res.* **32**, 285–300.

DUMORÉ, J. M., MERK, H. J. & PRINS, J. A. 1953 Heat transfer from water to ice by thermal convection. *Nature* **172**, 460–461.

EDE, A. J. 1951 Heat transfer by natural convection in refrigerated liquid. *Proc. 8th Int. Cong. Refrigeration, London*, p. 260. (See also The influence of anomalous expansion on natural convection in water. *Appl. Sci. Res.* **5** (1955), 458–460.)

FINE, R. A. & MILLERO, F. J. 1973 Compressibility of water as a function of temperature and pressure. *J. Chem. Phys.* **59**, 5529–5536.

FUJINO, K., LEWIS, E. L. & PERKIN, R. G. 1974 The freezing point of sea water at pressures up to 100 bars. *J. Geophys. Res.* **79**, 1792–1797.

GEBHART, B. 1971 *Heat Transfer*, 2nd edn. McGraw-Hill.

GEBHART, B. 1973 Boundary layer flows and instability in natural convection. *Adv. Heat Transfer* **9**, 273–348.

GEBHART, B. & MOLLENDORF, J. C. 1977 A new density relation for pure and saline water. *Deep-Sea Res.* **24**, 831–848.

GEBHART, B. & PERA, L. 1971 The nature of vertical natural convection flows resulting from the combined buoyancy effects of thermal and mass diffusion. *Int. J. Heat Mass Transfer* **14**, 2025–2050.

GOREN, S. L. 1966 On free convection in water at 4° C. *Chem. Engng Sci.* **21**, 515–518.

GOVINDARAJULU, T. 1970 Free convection flow of water at 4° C on vertical and horizontal plates. *Chem. Engng Sci.* **25**, 1827–1828.

JOSEPH, D. D. 1971 Stability of convection in containers of arbitrary shape. *J. Fluid Mech.* **47**, 257–282.

LORENZ, L. 1881 Über das Leitungsvermögen der Metalle für Wärme und Electricität. *Ann. Phys. Chem.* **13**, 582–606.

MERK, H. J. 1953 The influence of melting and anomalous expansion on the thermal convection in laminar boundary layers. *Appl. Sci. Res.* **4**, 435–452.

OBORIN, L. A. 1967 Special features of free convection in water at temperatures below 277 °K. *J. Engng Phys.* **13**, 429–442.

OBERBECK, A. 1879 Uber die Wärmeleitung der Flussigkeiten bei der Berüchsichtigung der Strömungen infolge von Temperaturdifferenzen. *Ann. Phys. Chem.* **7**, 271–292.

PERRY, J. H. 1963 *Chemical Engineers' Handbook*, 4th edn, § 3, p. 70. McGraw-Hill.

ROY, S. 1972 Free convection in liquids under maximum density conditions. *Indian J. Phys.* **46**, 245–249.

SCHECHTER, R. S. & ISBIN, H. S. 1958 Natural convection heat transfer in regions of maximum fluid density. *A.I.Ch.E. J.* **4**, 81–89.

SCHENK, J. & SCHENKELS, F. A. M. 1968 Thermal free convection from an ice sphere in water. *Appl. Sci. Res.* **19**, 465–476.

SOUNDALGEKAR, V. M. 1973 Laminar free convection flow of water at 4 °C from a vertical plate with variable wall temperature. *Chem. Engng Sci.* **28**, 307–309.

VANIER, C. R. & TIEN, C. 1967 Further work on free convection in water at 4 °C. *Chem. Engng Sci.* **22**, 1747–1751.

VANIER, C. R. & TIEN, C. 1968 Effect of maximum density and melting on natural convection heat transfer from a vertical plate. *Chem. Engng Prog. Symp. Ser.* **64**, 240–254.